

Structural ground states of $(A, A')\text{Cr}_2\text{O}_4$ ($A=\text{Mg}, \text{Zn}$; $A' = \text{Co}, \text{Cu}$) spinel solid solutions: Spin-Jahn-Teller and Jahn-Teller effects

Moureen C. Kemei,^{1,*} Stephanie L. Moffitt,¹ Lucy E. Darago,^{1,†} Ram Seshadri,^{1,†} Matthew R. Suchomel,^{2,‡} Daniel P. Shoemaker,^{3,§} Katharine Page,^{4,¶} and Joan Siewenie^{4,**}

¹*Materials Department and Materials Research Laboratory
University of California, Santa Barbara, CA, 93106, USA*

²*Advanced Photon Source, Argonne National Laboratory, Argonne IL, 60439, USA*

³*Department of Materials Science and Engineering
University of Illinois at Urbana-Champaign, Urbana IL 61801, USA*

⁴*Lujan Neutron Scattering Center, Los Alamos National Laboratory, Los Alamos, New Mexico 87545, USA*
(Dated: January 15, 2014)

We examine the effect of small amounts of magnetic substituents in the A sites of the frustrated spinels MgCr_2O_4 and ZnCr_2O_4 . Specifically we look for the effects of spin and lattice disorder on structural changes accompanying magnetic ordering in these compounds. Substitution of Co^{2+} on the non-magnetic Zn^{2+} site in $\text{Zn}_{1-x}\text{Co}_x\text{Cr}_2\text{O}_4$ where $0 < x \leq 0.2$ completely suppresses the spin-Jahn-Teller distortion of ZnCr_2O_4 although these systems remain frustrated, and magnetic ordering occurs at very low temperatures of $T < 20$ K. On the other hand, the substitution of Jahn-Teller active Cu^{2+} for Mg^{2+} and Zn^{2+} in $\text{Mg}_{1-x}\text{Cu}_x\text{Cr}_2\text{O}_4$ and $\text{Zn}_{1-x}\text{Cu}_x\text{Cr}_2\text{O}_4$ where $0 < x \leq 0.2$ induce Jahn-Teller ordering at temperatures well above the Néel temperatures of these solid solutions, and yet spin interactions remain frustrated with long-range magnetic ordering occurring below 20 K without any further lattice distortion. The Jahn-Teller distorted solid solutions $\text{Mg}_{1-x}\text{Cu}_x\text{Cr}_2\text{O}_4$ and $\text{Zn}_{1-x}\text{Cu}_x\text{Cr}_2\text{O}_4$ adopt the orthorhombic $Fddd$ structure of ferrimagnetic CuCr_2O_4 . Total neutron scattering studies of $\text{Zn}_{1-x}\text{Cu}_x\text{Cr}_2\text{O}_4$ suggest that there are local AO_4 distortions in these Cu^{2+} -containing solid solutions at room temperature and that these distortions become cooperative when average structure distortions occur. Magnetism evolves from compensated antiferromagnetism in MgCr_2O_4 and ZnCr_2O_4 to uncompensated antiferromagnetism with substitution of magnetic cations on the non-magnetic cation sites of these frustrated compounds. The sharp heat capacity anomalies associated with the first-order spin-Jahn-Teller transitions of MgCr_2O_4 and ZnCr_2O_4 become broad in $\text{Mg}_{1-x}\text{Cu}_x\text{Cr}_2\text{O}_4$, $\text{Zn}_{1-x}\text{Co}_x\text{Cr}_2\text{O}_4$, and $\text{Zn}_{1-x}\text{Cu}_x\text{Cr}_2\text{O}_4$ when $x > 0$. We present a temperature-composition phase diagram summarizing the structural ground states and magnetic properties of the studied spinel solid solutions.

PACS numbers: 61.50.Ks, 75.50.Ee, 75.47.Lx

Triangular lattice topologies are at the center of complex ground states in functional oxides as has been shown in the charge ordered triangular metallic AgNiO_2 where charge ordering rather than a Jahn-Teller distortion lifts orbital degeneracy¹ and in geometrically frustrated spin systems such as ZnCr_2O_4 where magnetic ordering is accompanied by a lattice distortion.² The ground states of the canonical spin frustrated systems ACr_2O_4 ($A = \text{Mg}$,³⁻⁶ Zn ,^{2,6-8} Cd ,^{5,9,10} and Hg ¹¹) have been extensively explored. To understand the degenerate ground states of ACr_2O_4 spinels, the effect of spin disorder on the magnetic properties of these systems has been investigated; spin disorder is introduced by substituting magnetic ions on the non-magnetic A sublattice of these materials.¹²⁻¹⁴ Similarly, the effect of low concentrations of magnetic vacancies on the Cr sublattice of $\text{ZnCr}_{2(1-x)}\text{Ga}_{2x}\text{O}_4$ has been studied showing that the freezing temperature of these systems for small x is independent of the spin vacancy concentration.¹⁵ However, the effect of spin and lattice disorder on the structural ground states of the canonical frustrated systems MgCr_2O_4 and ZnCr_2O_4 has so far not been studied.

Here, we study magnetic ordering and correlated or uncorrelated structural changes in MgCr_2O_4 and ZnCr_2O_4

when low concentrations of magnetic cations are substituted on the non-magnetic A site. MgCr_2O_4 and ZnCr_2O_4 are ideal candidates for the present study as they are: (i) Strongly frustrated with expected ordering temperatures of about 400 K yet suppressed antiferromagnetic ordering occurs below 15 K¹⁶ (ii) Their structural and magnetic ground states are strongly coupled with a lattice distortion occurring concomitantly with antiferromagnetic ordering.^{2,3,6} (iii) Finally, Cr^{3+} $3d^3$ strongly prefers the octahedral site where it has a non-degenerate electronic configuration thus enabling compositional variation only on the tetrahedral A site. The effect of spin disorder on the structural ground states of ZnCr_2O_4 is investigated by substituting magnetic Co^{2+} with a tetrahedral ionic radius of 0.58 Å for Zn^{2+} which has an ionic radius of 0.6 Å in tetrahedral coordination.¹⁷ The similarity in ionic radii between Co^{2+} and Zn^{2+} minimizes the effects of lattice distortion while allowing us to probe the effect of dilute A site spins on the structural ground states of ZnCr_2O_4 . Jahn-Teller active Cu^{2+} with an ionic radii of 0.57 Å is introduced to the A sites of MgCr_2O_4 and ZnCr_2O_4 to study the effect of both structural and spin disorder on the structural ground states of these systems.¹⁷ Mg^{2+} has a Shannon-Prewitt ionic

radius of 0.57 Å in tetrahedral coordination.¹⁷

This study is enabled by variable-temperature high-resolution synchrotron X-ray diffraction, which is a powerful tool for investigating the coupling of spin and lattice degrees of freedom in magnetic oxides. For example, it has been used to show that exchange striction drives further distortions to orthorhombic symmetry in the already Jahn-Teller distorted tetragonal spinels NiCr_2O_4 and CuCr_2O_4 .¹⁸ Similarly, high-resolution synchrotron X-ray diffraction revealed phase coexistence in the spin-Jahn-Teller phases of MgCr_2O_4 and ZnCr_2O_4 .⁶ Barton *et al.* have also shown a spin-driven rhombohedral to monoclinic structural distortion in $\text{Co}_{10}\text{Ge}_3\text{O}_{16}$.¹⁹

We show that $\geq 10\%$ Co^{2+} ions on the Zn^{2+} site of ZnCr_2O_4 suppress the structural distortion that accompanies antiferromagnetic ordering in ZnCr_2O_4 . We also find that concentrations $\geq 10\%$ of Jahn-Teller active Cu^{2+} on the Mg^{2+} site of MgCr_2O_4 and on the Zn^{2+} site of ZnCr_2O_4 induce average structure distortions at temperatures above the magnetic ordering temperature. The Jahn-Teller average structure distortion in $\text{Mg}_{1-x}\text{Cu}_x\text{Cr}_2\text{O}_4$ and $\text{Zn}_{1-x}\text{Cu}_x\text{Cr}_2\text{O}_4$ occurs at higher temperatures with increase in x . Despite the lattice distortions in $\text{Mg}_{1-x}\text{Cu}_x\text{Cr}_2\text{O}_4$ and $\text{Zn}_{1-x}\text{Cu}_x\text{Cr}_2\text{O}_4$ when $x \geq 0.1$, magnetic interactions remain frustrated and no further average structure distortions are observed at the Néel temperature. The Jahn-Teller distorted systems $\text{Mg}_{1-x}\text{Cu}_x\text{Cr}_2\text{O}_4$ and $\text{Zn}_{1-x}\text{Cu}_x\text{Cr}_2\text{O}_4$ when $x \geq 0.1$, are orthorhombic in the space group $Fddd$. In all the studied solid solutions, magnetism evolves from frustrated antiferromagnetism to glassy uncompensated antiferromagnetism.

I. METHODS

Powder samples of $\text{Zn}_{1-x}\text{Co}_x\text{Cr}_2\text{O}_4$, $\text{Mg}_{1-x}\text{Cu}_x\text{Cr}_2\text{O}_4$, and $\text{Zn}_{1-x}\text{Cu}_x\text{Cr}_2\text{O}_4$ were prepared using solid state preparation methods. The samples $\text{Mg}_{1-x}\text{Cu}_x\text{Cr}_2\text{O}_4$ were prepared from stoichiometric solution mixtures of the nitrates $\text{Mg}(\text{NO}_3)_2 \cdot 6\text{H}_2\text{O}$, $\text{Cu}(\text{NO}_3)_2 \cdot 6\text{H}_2\text{O}$, and $\text{Cr}(\text{NO}_3)_3 \cdot 9\text{H}_2\text{O}$. The nitrate precursor was calcined at temperatures between 700 °C and 1000 °C for 10 hours as reported by Shoemaker and Seshadri.²⁰ Powders of $\text{Zn}_{1-x}\text{Cu}_x\text{Cr}_2\text{O}_4$ were prepared from stoichiometric amounts of ZnO , CuO , and Cr_2O_3 that were ground, pressed into pellets, and calcined at 800 °C for 12 hours. These samples were reground, pressed into pellets, and annealed at 1000 °C for 48 hours followed by further annealing at 800 °C for 12 hours. Stoichiometric powders of $\text{Zn}_{1-x}\text{Co}_x\text{Cr}_2\text{O}_4$ were prepared from $\text{CoC}_2\text{O}_4 \cdot 2\text{H}_2\text{O}$, ZnO , and Cr_2O_3 . These powders were mixed, pressed into pellets, and calcined at 800 °C for 12 hours. The samples were then reground, pressed into pellets, and annealed at 1150 °C for 12 hours followed by further annealing at 800 °C for 24 hours. Samples were structurally characterized by high-resolution ($\delta Q/Q \leq 2 \times 10^{-4}$) variable-temperature

(6 K $\leq T \leq$ 300 K) synchrotron X-ray powder diffraction at beamline 11BM at the Advanced Photon Source, Argonne National Laboratory. Diffraction patterns were fit to structural models using the Rietveld method as implemented in the EXPGUI/GSAS software program.^{21,22} Crystal structures are visualized using the program VESTA.²³ Magnetic properties were measured using the Quantum Design MPMS 5XL superconducting quantum interference device (SQUID). Heat capacity measurements were performed using a Quantum Design Physical Properties Measurement System. Time-of-flight neutron scattering data was collected on the NPDF instrument at Los Alamos National Laboratory. The neutron pair distribution function (NPDF) with a maximum Q of 35 Å⁻¹ was processed using the PDFGETN program.²⁴ Least squares refinement of the NPDFs was performed using PDFGUI.²⁵

II. RESULTS AND DISCUSSION

A. $\text{Zn}_{1-x}\text{Co}_x\text{Cr}_2\text{O}_4$

ZnCr_2O_4 and CoCr_2O_4 are normal cubic spinels in the space group $Fd\bar{3}m$ at room temperature. These systems vary significantly in their magnetic properties, primarily due to the differences in properties of the A site cations. Zn^{2+} has the closed electron configuration $[\text{Ar}]3d^{10}$ which renders it magnetically inert. Direct antiferromagnetic Cr^{3+} - Cr^{3+} interactions in the pyrochlore Cr sublattice of ZnCr_2O_4 give rise to geometric frustration. A spin-Jahn-Teller distortion partially lifts spin frustration in ZnCr_2O_4 enabling the onset of antiferromagnetic order at the Néel temperature.^{2,8,26,27} The nuclear structure of the spin-Jahn-Teller phase of ZnCr_2O_4 has been extensively studied.^{2,6,8,27} Recently, our group has proposed a structural model of coexisting tetragonal $I4_1/amd$ and orthorhombic $Fddd$ phases for ZnCr_2O_4 .⁶ On the other hand, Co^{2+} has the electronic configuration $[\text{Ar}]3d^7$ with three unpaired spins that interact ferrimagnetically with Cr^{3+} through Co^{2+} -O- Cr^{3+} superexchange interactions. CoCr_2O_4 shows complex magnetic behavior; it undergoes a magnetic phase transition from a paramagnetic state to a ferrimagnetic long-range ordered state near 94 K.²⁸⁻³⁰ A recent report by Chang *et al.* shows long range spiral order in CoCr_2O_4 below 25 K with an incommensurate propagation vector and a transition at 14 K to commensurate spiral order.³¹ While no studies report a lowering of structural symmetry in CoCr_2O_4 , ultrasound propagation measurements performed on single crystals of CoCr_2O_4 by Tsurkan *et al.* show a field-induced structural distortion to cubic symmetry at high magnetic fields.³² CoCr_2O_4 exhibits spin charge coupling; the onset of incommensurate spiral order in CoCr_2O_4 is accompanied by a change in the dielectric constant.^{30,33} In addition, the dielectric constant shows magnetic field dependence below 95 K.³³ We examine the changes in structural ground states of ZnCr_2O_4 when 10% and 20%

Co^{2+} cations are substituted on the non-magnetic Zn^{2+} site.

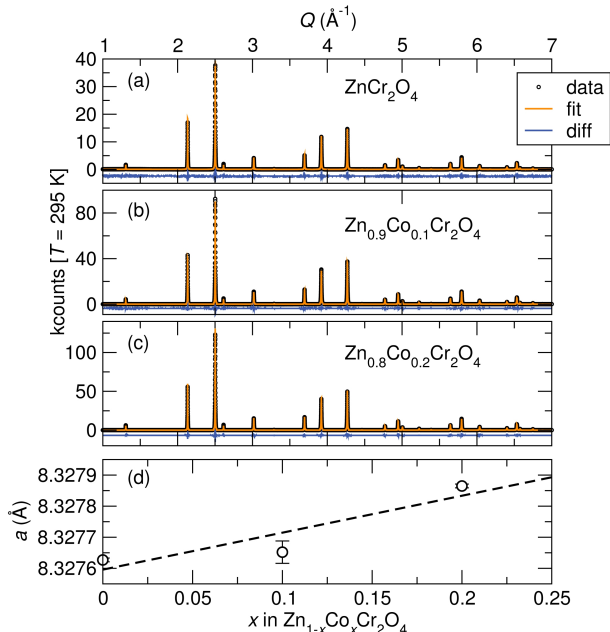


FIG. 1: (Color online) Room temperature synchrotron X-ray diffraction of the compounds (a) ZnCr_2O_4 , (b) $\text{Zn}_{0.9}\text{Co}_{0.1}\text{Cr}_2\text{O}_4$, and (c) $\text{Zn}_{0.8}\text{Co}_{0.2}\text{Cr}_2\text{O}_4$. All samples are well described in the cubic space group $Fd\bar{3}m$ and no impurity peaks are observed. (d) A unit cell expansion occurs with substitution of Co^{2+} for Zn^{2+} in $\text{Zn}_{1-x}\text{Co}_x\text{Cr}_2\text{O}_4$. The dashed line is a linear fit to the lattice parameters of $\text{Zn}_{1-x}\text{Co}_x\text{Cr}_2\text{O}_4$.

TABLE I: Magnetic parameters of $\text{Zn}_{1-x}\text{Co}_x\text{Cr}_2\text{O}_4$.

	T_N (K)	$\mu_{eff}(\mu_B)$	$\mu_{calc}(\mu_B)$	$\Theta_{CW}(\text{K})$
ZnCr_2O_4	12.3	5.2	5.48	-288
$\text{Zn}_{0.9}\text{Co}_{0.1}\text{Cr}_2\text{O}_4$	9	5.4	5.61	-350
$\text{Zn}_{0.8}\text{Co}_{0.2}\text{Cr}_2\text{O}_4$	11	5.6	5.74	-369

At room temperature, the prepared compounds $\text{Zn}_{1-x}\text{Co}_x\text{Cr}_2\text{O}_4$ where $x \leq 0.2$ are cubic spinels in the space group $Fd\bar{3}m$ (Fig. 1 and Table IV of the appendix). The similarity in the tetrahedral ionic radii of Co^{2+} and Zn^{2+} allows the entire solid solution $\text{Zn}_{1-x}\text{Co}_x\text{Cr}_2\text{O}_4$ to retain cubic $Fd\bar{3}m$ symmetry at room temperature.¹² Despite the smaller ionic radius of Co^{2+} , a unit cell expansion occurs with substitution of Co^{2+} for Zn^{2+} in $\text{Zn}_{1-x}\text{Co}_x\text{Cr}_2\text{O}_4$. The observed unit cell expansion has been previously reported and is attributed to higher cation-cation repulsion with increasing substitution of the more ionic Co^{2+} for Zn^{2+} in $\text{Zn}_{1-x}\text{Co}_x\text{Cr}_2\text{O}_4$.¹²

Antiferromagnetic interactions of the geometrically frustrated spinel ZnCr_2O_4 [Fig. 2 (a)] evolve to uncompensated antiferromagnetic interactions in $\text{Zn}_{0.8}\text{Co}_{0.2}\text{Cr}_2\text{O}_4$ [Fig. 2 (c)]. Compensated interactions of ZnCr_2O_4 are illustrated by the upward turn of the inverse susceptibility below the magnetic ordering

temperature and this contrasts with uncompensated antiferromagnetic interactions in $\text{Zn}_{0.8}\text{Co}_{0.2}\text{Cr}_2\text{O}_4$ where magnetic ordering yields a downward turn of the inverse susceptibility. An increase in the number of magnetic interactions is expected in $\text{Zn}_{1-x}\text{Co}_x\text{Cr}_2\text{O}_4$ with increase in x . Accordingly, Curie-Weiss fitting in the paramagnetic regime ($300 \leq T \leq 390$ K) of $\text{Zn}_{1-x}\text{Co}_x\text{Cr}_2\text{O}_4$ yields an increasing Θ_{CW} with x (Table I). Similarly, the expected increase in effective moment with Co^{2+} substitution is also observed (Table I). When spins are substituted on the non-magnetic A sites of ACr_2O_4 spinels at concentrations greater than 20%, spin frustration is lifted.^{12–14} However, at dilute A site spin concentrations, disorder in the spin interactions has been shown to further suppress magnetic ordering.^{12–14} Due to the disorder in spin interactions, magnetic ordering in $\text{Zn}_{0.9}\text{Co}_{0.1}\text{Cr}_2\text{O}_4$ and $\text{Zn}_{0.8}\text{Co}_{0.2}\text{Cr}_2\text{O}_4$ occurs at lower temperatures compared to ZnCr_2O_4 (Table I).

Antiferromagnetic order in ZnCr_2O_4 occurs concurrently with a structural distortion (middle panel of Fig. 2). The structural ground state of ZnCr_2O_4 has been extensively investigated and a recent report from our group shows that the spin-Jahn-Teller phase of ZnCr_2O_4 is best described by the combination of tetragonal $I4_1/amd$ and orthorhombic $Fddd$ space groups.^{6,8,27} While ZnCr_2O_4 exhibits a clear lattice distortion at the Néel temperature, the cubic $Fd\bar{3}m$ (800) reflection for samples $x = 0.1$ and $x = 0.2$ shows no divergence illustrating the complete suppression of long-range structural distortion in these materials. As a result, the average nuclear structures of $\text{Zn}_{0.9}\text{Co}_{0.1}\text{Cr}_2\text{O}_4$ and $\text{Zn}_{0.8}\text{Co}_{0.2}\text{Cr}_2\text{O}_4$ near 5 K are well modeled by the cubic space group $Fd\bar{3}m$ as illustrated in Fig. 3. However, a clear peak broadening of the (800) reflection occurs near 5 K in $\text{Zn}_{0.9}\text{Co}_{0.1}\text{Cr}_2\text{O}_4$ and $\text{Zn}_{0.8}\text{Co}_{0.2}\text{Cr}_2\text{O}_4$ as shown in Fig. 3 (c) and (f) respectively. This broadening is indicative of higher strain at low temperatures that can result from local distortions in these materials. The structural parameters of $\text{Zn}_{0.9}\text{Co}_{0.1}\text{Cr}_2\text{O}_4$ and $\text{Zn}_{0.8}\text{Co}_{0.2}\text{Cr}_2\text{O}_4$ are tabulated in Table IV of the appendix.

The spin-Jahn-Teller distortion of ZnCr_2O_4 yields a sharp heat capacity anomaly at T_N [Fig. 2 (d)]. This heat capacity anomaly is slightly suppressed in $\text{Zn}_{0.9}\text{Co}_{0.1}\text{Cr}_2\text{O}_4$ and it becomes very broad in $\text{Zn}_{0.8}\text{Co}_{0.2}\text{Cr}_2\text{O}_4$ [Fig. 2 (e) and (f)]. The suppression of the heat capacity anomalies in $\text{Zn}_{0.9}\text{Co}_{0.1}\text{Cr}_2\text{O}_4$ and $\text{Zn}_{0.8}\text{Co}_{0.2}\text{Cr}_2\text{O}_4$ shows that these systems host residual spin and structural disorder.

We have shown the differences in structural ground state when $\geq 10\%$ of Co^{2+} are substituted on the non-magnetic A site of ZnCr_2O_4 . The structural distortion that accompanies magnetic ordering in ZnCr_2O_4 is completely suppressed even for only 10% Co^{2+} substitution in $\text{Zn}_{0.9}\text{Co}_{0.1}\text{Cr}_2\text{O}_4$. This suggests that random Co-O-Cr superexchange interactions in $\text{Zn}_{1-x}\text{Co}_x\text{Cr}_2\text{O}_4$, partially break the spin ground state degeneracy of these systems, allowing the onset of a magnetic ground state without the

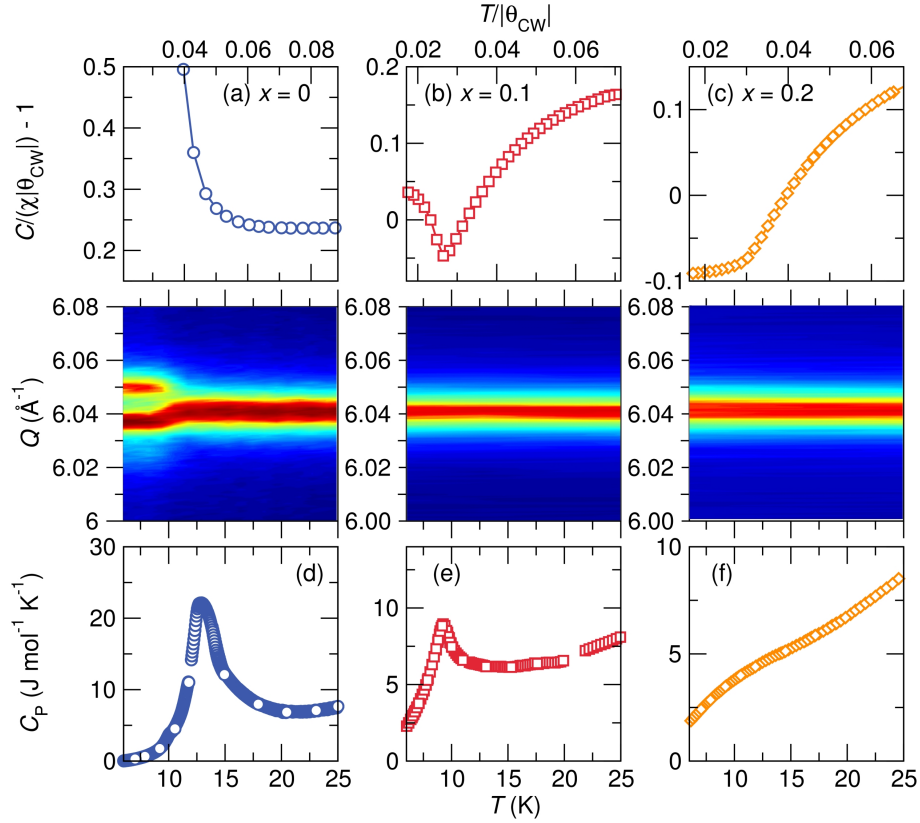


FIG. 2: (Color online) Suppression of the spin-Jahn-Teller distortion in $\text{Zn}_{1-x}\text{Co}_x\text{Cr}_2\text{O}_4$ with increase in x . (a) Inverse scaled magnetic susceptibility as a function of temperature for (a) ZnCr_2O_4 , (b) $\text{Zn}_{0.9}\text{Co}_{0.1}\text{Cr}_2\text{O}_4$, and (c) $\text{Zn}_{0.8}\text{Co}_{0.2}\text{Cr}_2\text{O}_4$ measured in a 1000 Oe field. Compensated antiferromagnetic interactions of ZnCr_2O_4 shown by the upward turn of the inverse susceptibility below the magnetic ordering temperature become uncompensated with the introduction of Co^{2+} in place of Zn^{2+} as illustrated by downward turn of the susceptibility of $\text{Zn}_{0.8}\text{Co}_{0.2}\text{Cr}_2\text{O}_4$ below the Néel temperature. The middle panel shows variable-temperature high-resolution X-ray powder diffraction of the cubic (800) reflection. Geometric frustration in ZnCr_2O_4 drives the lattice distortion shown by the splitting of the (800) reflection at the Néel temperature (12.3 K) of ZnCr_2O_4 . The spin-Jahn-Teller distortion of ZnCr_2O_4 is suppressed even when only 10% Co^{2+} cations are substituted for Zn^{2+} . (d) The sharp heat capacity anomaly observed at the spin-Jahn-Teller distortion temperature of ZnCr_2O_4 is suppressed in $\text{Zn}_{0.9}\text{Co}_{0.1}\text{Cr}_2\text{O}_4$ (e) and strongly suppressed in $\text{Zn}_{0.8}\text{Co}_{0.2}\text{Cr}_2\text{O}_4$ (f).

need for a long range structural distortion. It is also plausible that random Co-O-Cr superexchange interactions could be disrupting the coherency of Cr-Cr exchange coupling paths thus inhibiting spin-Jahn-Teller distortions in $\text{Zn}_{0.9}\text{Co}_{0.1}\text{Cr}_2\text{O}_4$ and $\text{Zn}_{0.8}\text{Co}_{0.2}\text{Cr}_2\text{O}_4$. Small substitutions of Co^{2+} for Mg^{2+} will likely suppress the Spin-Jahn-Teller distortion of MgCr_2O_4 ; this is supported by the similar structural effects of Cu^{2+} substitutions for Mg^{2+} and Zn^{2+} in MgCr_2O_4 and ZnCr_2O_4 as discussed in the following sections.

B. $\text{Mg}_{1-x}\text{Cu}_x\text{Cr}_2\text{O}_4$

We examine the effect of both spin and lattice disorder on the spin-Jahn-Teller ground state of MgCr_2O_4 by substituting $\geq 10\%$ of Jahn-Teller active Cu^{2+} for Mg^{2+} . At room temperature the normal spinels MgCr_2O_4 and CuCr_2O_4 have different structural ground states;

MgCr_2O_4 is cubic while CuCr_2O_4 is tetragonal. The tetragonal structure of CuCr_2O_4 results from cooperative Jahn-Teller ordering of CuO_4 tetrahedra at $T = 853\text{ K}$.³⁴ MgCr_2O_4 is a frustrated antiferromagnet, and its transition to an ordered magnetic state at $T_N = 12.9\text{ K}$ is accompanied by a structural distortion.^{3,4} The spin-Jahn-Teller distorted phase of MgCr_2O_4 had been previously described by the tetragonal $I4_1/amd$ structure,^{3,4} but we have recently shown that this system consists of coexisting tetragonal $I4_1/amd$ and orthorhombic $Fddd$ phases.⁶ CuCr_2O_4 is ferrimagnetic, with magnetic Cu^{2+} and Cr^{3+} sublattices contributing to a non-collinear magnetic structure where two canted Cr^{3+} sublattices yield a magnetic moment that is partially compensated by the Cu^{2+} sublattice at $T_N = 135\text{ K}$.³⁵ In addition to the high temperature Jahn-Teller driven cubic-tetragonal phase transition, CuCr_2O_4 undergoes yet another structural distortion from tetragonal $I4_1/amd$ to orthorhombic $Fddd$ symmetry near 130 K

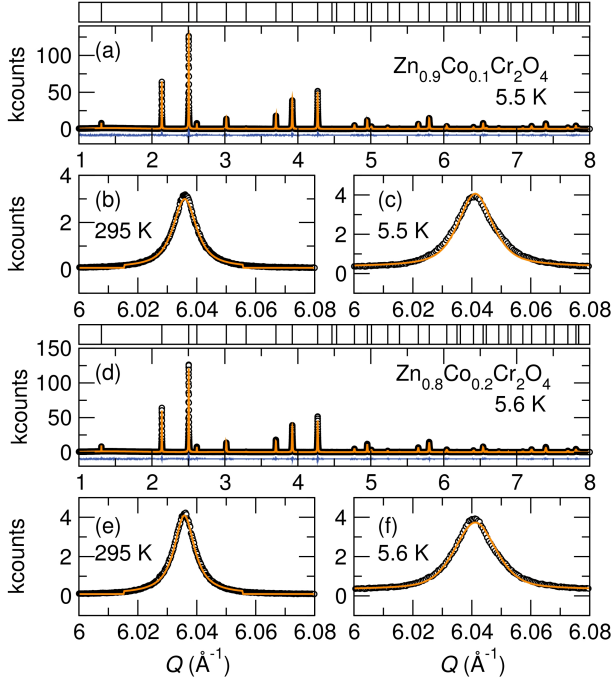


FIG. 3: (Color online) Low temperature synchrotron X-ray diffraction of (a) $\text{Zn}_{0.9}\text{Co}_{0.1}\text{Cr}_2\text{O}_4$, and (d) $\text{Zn}_{0.8}\text{Co}_{0.2}\text{Cr}_2\text{O}_4$ modeled to the cubic space group $Fd\bar{3}m$. The (800) reflections of $\text{Zn}_{0.9}\text{Co}_{0.1}\text{Cr}_2\text{O}_4$ and $\text{Zn}_{0.8}\text{Co}_{0.2}\text{Cr}_2\text{O}_4$ at room temperature are shown here in (b) and (e) respectively and near 5 K in (c) and (f) respectively. A broadening of the (800) reflection is observed at low temperature in $\text{Zn}_{0.9}\text{Co}_{0.1}\text{Cr}_2\text{O}_4$ and $\text{Zn}_{0.8}\text{Co}_{0.2}\text{Cr}_2\text{O}_4$.

TABLE II: Magnetic parameters of $\text{Mg}_{1-x}\text{Cu}_x\text{Cr}_2\text{O}_4$.

	T_N (K)	$\mu_{exp}(\mu_B)$	$\mu_{calc}(\mu_B)$	Θ_{CW} (K)
MgCr_2O_4	12.9	5.2	5.47	-368
$\text{Mg}_{0.9}\text{Cu}_{0.1}\text{Cr}_2\text{O}_4$	11	5.3	5.50	-361
$\text{Mg}_{0.8}\text{Cu}_{0.2}\text{Cr}_2\text{O}_4$	15	5.2	5.53	-329

due to magnetostructural coupling.¹⁸

The prepared spinel solid solutions $\text{Mg}_{1-x}\text{Cu}_x\text{Cr}_2\text{O}_4$ where $x \leq 0.2$ are cubic with the space group $Fd\bar{3}m$ at room temperature [Fig. 4 (a), (b), and (c)]. While tetrahedral Mg^{2+} and Cu^{2+} have identical Shannon-Prewitt ionic radii, we observe a lattice contraction with increase in Cu^{2+} , following Vegard's law [Figure 4 (d)]. This decrease in lattice constant with Cu^{2+} substitution is consistent with the earlier work by Shoemaker and Seshadri²⁰ and with the smaller pseudocubic cell volume of CuCr_2O_4 (566.38 \AA^3)¹⁸ compared with that of MgCr_2O_4 (579.017 \AA^3) at room temperature.⁶ The structural parameters of $\text{Mg}_{1-x}\text{Cu}_x\text{Cr}_2\text{O}_4$ for $x = 0.1$ and 0.2 at 300 K are tabulated in Table. V of the appendix.

The evolution of magnetism in $\text{Mg}_{1-x}\text{Cu}_x\text{Cr}_2\text{O}_4$ where $x \leq 0.2$, is similar to that observed in $\text{Zn}_{1-x}\text{Co}_x\text{Cr}_2\text{O}_4$; frustrated antiferromagnetism in MgCr_2O_4 evolves to uncompensated antiferromag-

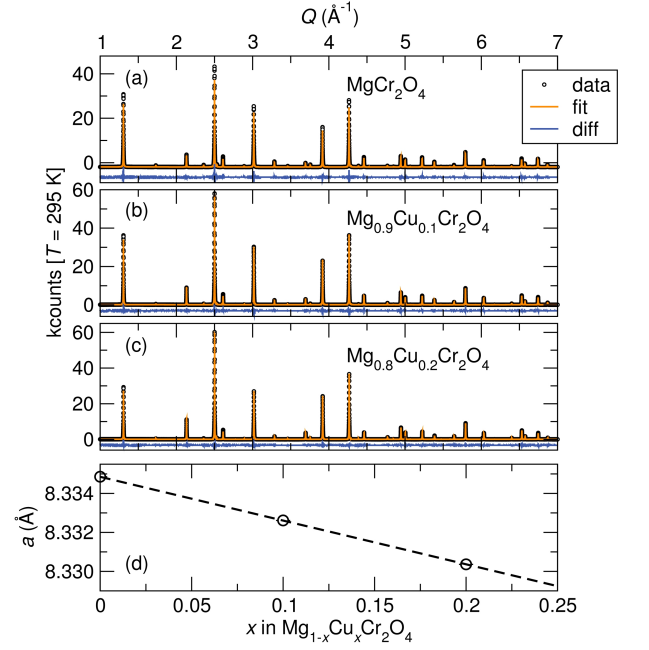


FIG. 4: (Color online) Rietveld refinement of room temperature high resolution synchrotron X-ray powder diffraction of (a) MgCr_2O_4 (b) $\text{Mg}_{0.9}\text{Cu}_{0.1}\text{Cr}_2\text{O}_4$ and (c) $\text{Mg}_{0.8}\text{Cu}_{0.2}\text{Cr}_2\text{O}_4$ to the cubic space group $Fd\bar{3}m$. All samples show a very small Cr_2O_3 impurity with concentrations $< 1\%$ in all samples. (d) The cubic lattice constant in $\text{Mg}_{1-x}\text{Cu}_x\text{Cr}_2\text{O}_4$ decreases linearly with increase in Cu^{2+} concentration. Error bars are smaller than data symbols.

netism in $\text{Mg}_{0.8}\text{Cu}_{0.2}\text{Cr}_2\text{O}_4$ [Fig. 5 (a), (b), and (c)]. Antiferromagnetic ordering in $\text{Mg}_{0.9}\text{Cu}_{0.1}\text{Cr}_2\text{O}_4$ occurs at a lower temperature than in MgCr_2O_4 due to dilute $J_{Cu-O-Cr}$ couplings interfering with J_{Cr-Cr} couplings (Table II). However, the increase in Cu^{2+} concentration in $\text{Mg}_{0.8}\text{Cu}_{0.2}\text{Cr}_2\text{O}_4$ yields a higher magnetic ordering temperature and this is consistent with the findings that sufficient magnetic A site spins lift frustration in geometrically frustrated ACr_2O_4 spinels.¹²⁻¹⁴ Curie-Weiss fitting in the paramagnetic regime $300 \text{ K} \leq T \leq 390 \text{ K}$, of $\text{Mg}_{1-x}\text{Cu}_x\text{Cr}_2\text{O}_4$ yields a slight increase in the effective moment of $\text{Mg}_{0.9}\text{Cu}_{0.1}\text{Cr}_2\text{O}_4$ and a weakening of the overall strength of magnetic interactions shown by the decrease in the magnitude of Θ_{CW} (Table II). Weaker antiferromagnetic interactions with Cu^{2+} substitution are attributed to the effects of spin disorder due to dilute A site spins. The decrease in Θ_{CW} in $\text{Mg}_{1-x}\text{Cu}_x\text{Cr}_2\text{O}_4$ with increase in x contrasts with the increase in Θ_{CW} in $\text{Zn}_{1-x}\text{Co}_x\text{Cr}_2\text{O}_4$ with increase in x ; this difference is attributed to the higher spin of Co^{2+} $3d^7 s = \frac{3}{2}$ compared to Cu^{2+} $3d^9 s = \frac{1}{2}$. The higher spin of Co^{2+} contributes to stronger magnetic interactions in $\text{Zn}_{1-x}\text{Co}_x\text{Cr}_2\text{O}_4$.

Structural distortions are observed in all compounds $\text{Mg}_{1-x}\text{Cu}_x\text{Cr}_2\text{O}_4$ when $x \leq 0.2$. The spin-Jahn-Teller distortion of MgCr_2O_4 is illustrated by the splitting of the (800) reflection to several low temperature peaks (Leftmost middle panel of Fig. 5). While degener-

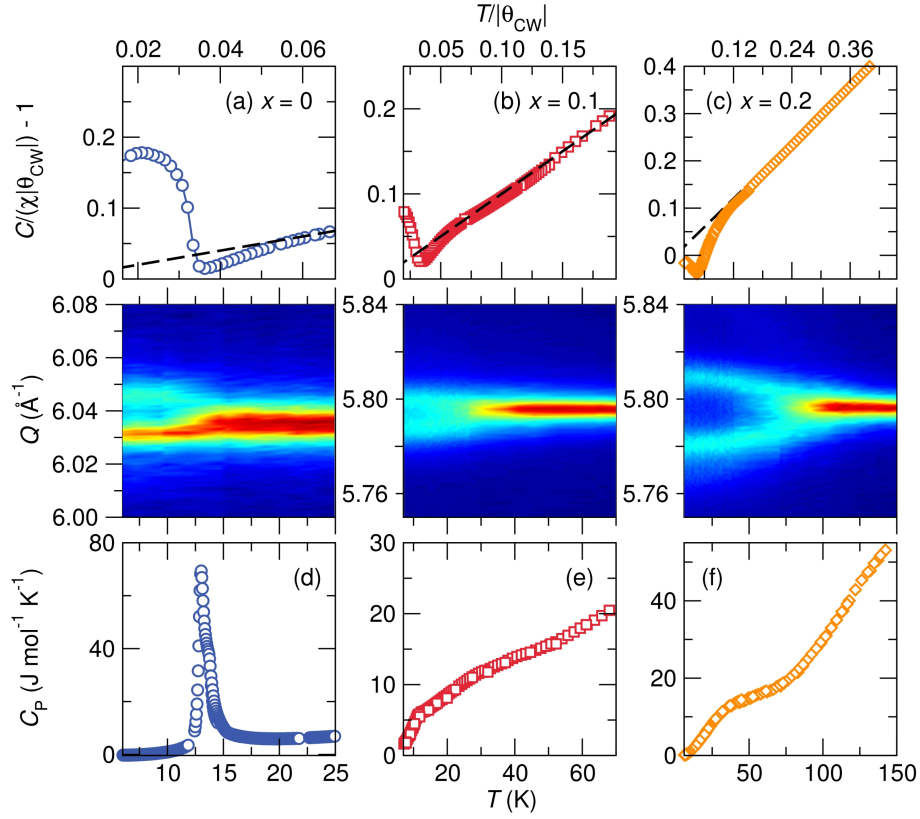


FIG. 5: (Color online) Spin-Jahn-Teller and Jahn-Teller ordering in $\text{Mg}_{1-x}\text{Cu}_x\text{Cr}_2\text{O}_4$. The top panel shows the scaled inverse susceptibility of MgCr_2O_4 (a), $\text{Mg}_{0.9}\text{Cu}_{0.1}\text{Cr}_2\text{O}_4$ (b) and $\text{Mg}_{0.8}\text{Cu}_{0.2}\text{Cr}_2\text{O}_4$ (c) measured in a 1000 Oe field. Compensated antiferromagnetic interactions in MgCr_2O_4 (a) and $\text{Mg}_{0.9}\text{Cu}_{0.1}\text{Cr}_2\text{O}_4$ (b) evolve to uncompensated antiferromagnetic interactions in $\text{Mg}_{0.8}\text{Cu}_{0.2}\text{Cr}_2\text{O}_4$ (c). Geometric frustration of spins in MgCr_2O_4 drives a structural distortion at $T_N = 12.9$ K that is indicated by the splitting of the high symmetry (800) reflection. Cooperative Jahn-Teller ordering spurs average structure distortions in $\text{Mg}_{0.9}\text{Cu}_{0.1}\text{Cr}_2\text{O}_4$ at $T \sim 35$ K and $\text{Mg}_{0.8}\text{Cu}_{0.2}\text{Cr}_2\text{O}_4$ at $T \sim 110$ K. The structural distortions in $\text{Mg}_{0.9}\text{Cu}_{0.1}\text{Cr}_2\text{O}_4$ and $\text{Mg}_{0.8}\text{Cu}_{0.2}\text{Cr}_2\text{O}_4$ are decoupled from the magnetism and no further structural distortions occur near the Néel temperature of these compounds although they exhibit spin frustration. (d) There is a sharp heat capacity anomaly at the Néel temperature of MgCr_2O_4 with a shoulder feature plausibly indicating a slight separation in temperature of the magnetic and structural transitions. (e) $\text{Mg}_{0.9}\text{Cu}_{0.1}\text{Cr}_2\text{O}_4$ shows a broad heat capacity anomaly with a kink at T_N . (f) Similarly, $\text{Mg}_{0.8}\text{Cu}_{0.2}\text{Cr}_2\text{O}_4$ shows a broad heat capacity peak in the temperature range $6 \text{ K} \leq T \leq 80 \text{ K}$.

acy in spin ground states drives the structural distortion in MgCr_2O_4 , degeneracy in the orbital configurations of tetrahedral Cu^{2+} drive Jahn-Teller distortions in $\text{Mg}_{0.9}\text{Cu}_{0.1}\text{Cr}_2\text{O}_4$ and $\text{Mg}_{0.8}\text{Cu}_{0.2}\text{Cr}_2\text{O}_4$ at 35 K and 110 K respectively. The middle panel of figure 5 shows the splitting of the coincident (731) and (553) reflections in $\text{Mg}_{0.9}\text{Cu}_{0.1}\text{Cr}_2\text{O}_4$ and $\text{Mg}_{0.8}\text{Cu}_{0.2}\text{Cr}_2\text{O}_4$. The Jahn-Teller distortion increases with Cu^{2+} concentration as shown by the larger separation between the low-temperature reflections of $\text{Mg}_{0.8}\text{Cu}_{0.2}\text{Cr}_2\text{O}_4$ and the onset of this distortion at higher temperature in this compound. We note that magnetic transitions do not accompany the structural distortions of $\text{Mg}_{0.9}\text{Cu}_{0.1}\text{Cr}_2\text{O}_4$ and $\text{Mg}_{0.8}\text{Cu}_{0.2}\text{Cr}_2\text{O}_4$. The Jahn-Teller phases of $\text{Mg}_{0.9}\text{Cu}_{0.1}\text{Cr}_2\text{O}_4$ and $\text{Mg}_{0.8}\text{Cu}_{0.2}\text{Cr}_2\text{O}_4$ are well modeled by the orthorhombic $Fddd$ structure (Fig. 6) that is ascribed to CuCr_2O_4 following its magnetostructural distortion.¹⁸ An important difference between CuCr_2O_4 and these systems studied here is that the orthorhom-

bic structure of CuCr_2O_4 occurs due to magnetostructural coupling¹⁸ while the orthorhombic structure of $\text{Mg}_{0.9}\text{Cu}_{0.1}\text{Cr}_2\text{O}_4$ and $\text{Mg}_{0.8}\text{Cu}_{0.2}\text{Cr}_2\text{O}_4$ occurs in the paramagnetic regime driven primarily by cooperative Jahn-Teller ordering.

The spin-Jahn-Teller distortion of MgCr_2O_4 results in a sharp heat capacity anomaly with a slight shoulder feature [Fig. 5 (d)]. The shoulder feature is likely due to a slight separation in temperature of the magnetic and structural changes. The onset of heat capacity changes in $\text{Mg}_{0.9}\text{Cu}_{0.1}\text{Cr}_2\text{O}_4$ and $\text{Mg}_{0.8}\text{Cu}_{0.2}\text{Cr}_2\text{O}_4$ occur at high temperatures where structural changes begin and they persist to low temperatures where magnetic ordering occurs [Fig. 5 (e) and (f)].

While the substitution of Co^{2+} for Zn^{2+} suppresses spin-Jahn-Teller distortion in ZnCr_2O_4 , $\geq 10\%$ substitution of Jahn-Teller active Cu^{2+} for Mg^{2+} induces structural distortions in $\text{Mg}_{0.9}\text{Cu}_{0.1}\text{Cr}_2\text{O}_4$ and $\text{Mg}_{0.8}\text{Cu}_{0.2}\text{Cr}_2\text{O}_4$ at temperatures above the mag-

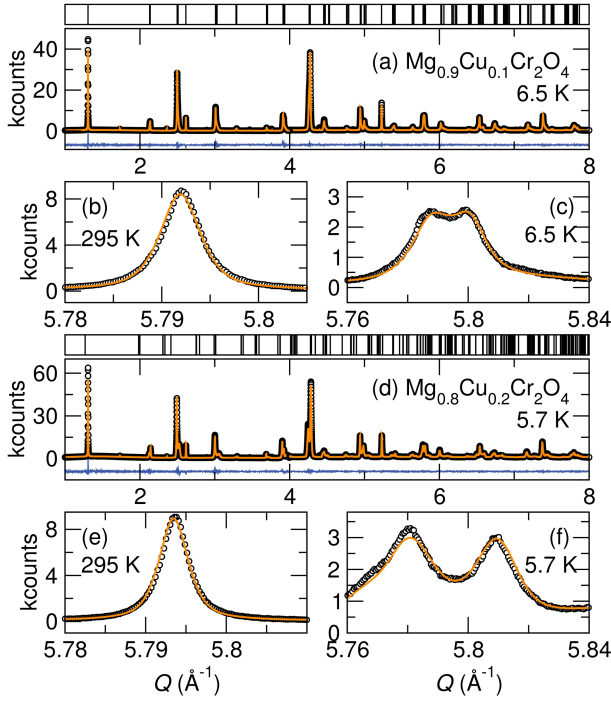


FIG. 6: (Color online) Low temperature structures of (a) $\text{Mg}_{0.9}\text{Cu}_{0.1}\text{Cr}_2\text{O}_4$ and (d) $\text{Mg}_{0.8}\text{Cu}_{0.2}\text{Cr}_2\text{O}_4$ indexed to the orthorhombic $Fddd$ structure. Data is shown in black, the structural model in orange and the difference between the structural model and the data is in blue. Below the respective Jahn-Teller ordering temperatures of $\text{Mg}_{0.9}\text{Cu}_{0.1}\text{Cr}_2\text{O}_4$ and $\text{Mg}_{0.8}\text{Cu}_{0.2}\text{Cr}_2\text{O}_4$, the coincident (731) and (553) reflections shown in (b) and (c) split into several reflections as shown in (e) and (f).

netic ordering temperatures of these compounds. The structural distortions in $\text{Mg}_{0.9}\text{Cu}_{0.1}\text{Cr}_2\text{O}_4$ and $\text{Mg}_{0.8}\text{Cu}_{0.2}\text{Cr}_2\text{O}_4$ affect the pyrochlore Cr sublattice; while there is only one Cr-Cr bond length at room temperature in the cubic phases of these systems, there are three Cr-Cr bond lengths in the orthorhombic phases of these materials. Surprisingly, spin interactions remain frustrated in $\text{Mg}_{0.9}\text{Cu}_{0.1}\text{Cr}_2\text{O}_4$ and $\text{Mg}_{0.8}\text{Cu}_{0.2}\text{Cr}_2\text{O}_4$ with magnetic ordering occurring below 18 K despite the presence of distortions in the pyrochlore Cr sublattice of these materials at temperatures above their Néel temperatures. No further structural distortions are observed in $\text{Mg}_{0.9}\text{Cu}_{0.1}\text{Cr}_2\text{O}_4$ and $\text{Mg}_{0.8}\text{Cu}_{0.2}\text{Cr}_2\text{O}_4$ near the Néel temperature.

C. $\text{Zn}_{1-x}\text{Cu}_x\text{Cr}_2\text{O}_4$

We examine the effect of Cu^{2+} substitutions for Zn^{2+} on the spin-Jahn-Teller distortion of ZnCr_2O_4 . All prepared samples $\text{Zn}_{1-x}\text{Cu}_x\text{Cr}_2\text{O}_4$ where $x \leq 0.2$ are cubic spinels in the space group $Fd\bar{3}m$ at room temperature as shown in Fig. 7. Like in the solid solutions $\text{Mg}_{1-x}\text{Cu}_x\text{Cr}_2\text{O}_4$, the substitution of Cu^{2+} for Zn^{2+} re-

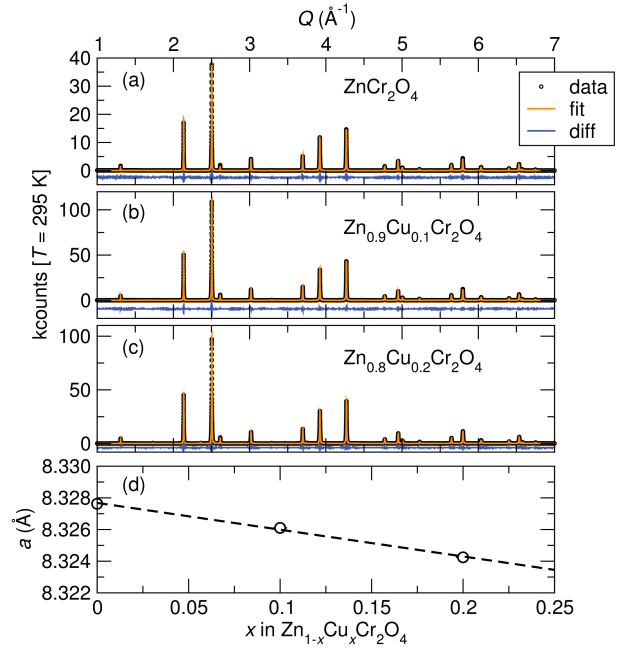


FIG. 7: (Color online) High resolution synchrotron X-ray powder diffraction of the systems (a) ZnCr_2O_4 (b) $\text{Zn}_{0.9}\text{Cu}_{0.1}\text{Cr}_2\text{O}_4$ and (c) $\text{Zn}_{0.8}\text{Cu}_{0.2}\text{Cr}_2\text{O}_4$ measured at room temperature. All compounds are well indexed by the cubic space group $Fd\bar{3}m$. (d) A linear decrease of the cubic lattice constant occurs with Cu^{2+} substitution for Zn^{2+} . Error bars are smaller than data symbols.

sults in a steady decrease of the lattice constant [Fig. 7 (d)]. This lattice decrease is in good agreement with the smaller cell volume of CuCr_2O_4 (566.38 \AA^3)¹⁸ at room temperature compared to ZnCr_2O_4 (577.520 \AA^3).⁶ The structural parameters of $\text{Zn}_{1-x}\text{Cu}_x\text{Cr}_2\text{O}_4$ are tabulated in Table VI of the appendix.

Compensated antiferromagnetic interactions in ZnCr_2O_4 and $\text{Zn}_{0.9}\text{Cu}_{0.1}\text{Cr}_2\text{O}_4$ evolve to uncompensated antiferromagnetic interactions in $\text{Zn}_{0.8}\text{Cu}_{0.2}\text{Cr}_2\text{O}_4$ [Figure 8(a), (b), and (c)]. The onset of magnetic ordering in $\text{Zn}_{0.9}\text{Cu}_{0.1}\text{Cr}_2\text{O}_4$ occurs at lower temperatures than in ZnCr_2O_4 due to disorder arising from dilute A site spins while $\text{Zn}_{0.8}\text{Cu}_{0.2}\text{Cr}_2\text{O}_4$ shows the highest ordering temperature of the studied $\text{Zn}_{1-x}\text{Cu}_x\text{Cr}_2\text{O}_4$ compounds (Table III). A slight decrease in the effective moment is observed with Cu^{2+} substitution in ZnCr_2O_4 and this is attributed to the presence of short range spin interactions in the paramagnetic regime contributing to the underestimation of the effective moment (Table III). As observed in $\text{Mg}_{1-x}\text{Cu}_x\text{Cr}_2\text{O}_4$, a decrease in the magnitude of Θ_{CW} occurs in $\text{Zn}_{1-x}\text{Cu}_x\text{Cr}_2\text{O}_4$ with increase in x suggesting that dilute Cu^{2+} substitutions weaken the overall strength of magnetic interactions in MgCr_2O_4 and ZnCr_2O_4 .

Geometric spin frustration drives a lattice distortion at the antiferromagnetic ordering temperature of ZnCr_2O_4 while Jahn-Teller distortion of tetrahedral Cu^{2+} in $\text{Zn}_{1-x}\text{Cu}_x\text{Cr}_2\text{O}_4$ drive structural distortions

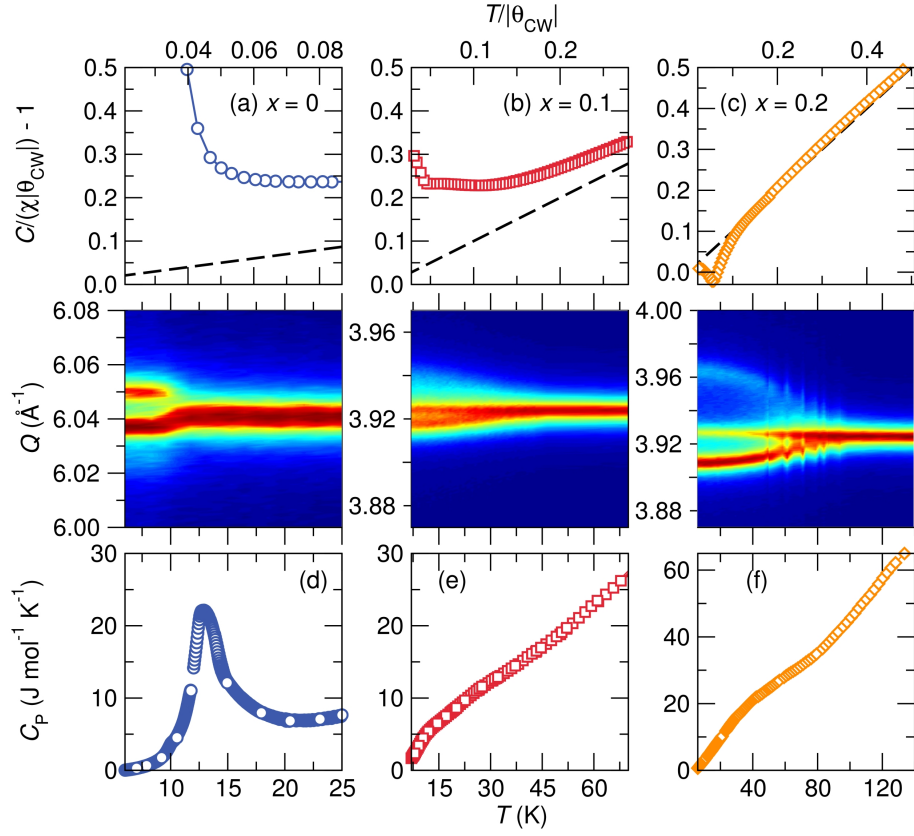


FIG. 8: (Color online) Spin-Jahn Teller and Jahn-Teller distortions in $\text{Zn}_{1-x}\text{Cu}_x\text{Cr}_2\text{O}_4$. The top panel shows inverse scaled susceptibility measurements of $\text{Zn}_{1-x}\text{Cu}_x\text{Cr}_2\text{O}_4$ measured under a 1000 Oe field. Compensated antiferromagnetism is observed in ZnCr_2O_4 (a) and $\text{Zn}_{0.9}\text{Cu}_{0.1}\text{Cr}_2\text{O}_4$ (b) below the Néel temperature while $\text{Zn}_{0.8}\text{Cu}_{0.2}\text{Cr}_2\text{O}_4$ (c) shows uncompensated antiferromagnetism. A lattice distortion accompanies magnetic ordering in ZnCr_2O_4 as shown by the splitting of the high symmetry (800) reflection at the Néel temperature. Jahn-Teller active Cu^{2+} on the A sites of $\text{Zn}_{0.9}\text{Cu}_{0.1}\text{Cr}_2\text{O}_4$ and $\text{Zn}_{0.8}\text{Cu}_{0.2}\text{Cr}_2\text{O}_4$ drive lattice distortions at approximately 45 K and 110 K respectively, where the coincident (511) and (333) reflections split into several low temperature reflections. There is a large heat capacity anomaly at the spin-Jahn-Teller distortion temperature of ZnCr_2O_4 (d). Broad heat capacity anomalies are observed in $\text{Zn}_{0.9}\text{Cu}_{0.1}\text{Cr}_2\text{O}_4$ (e) and $\text{Zn}_{0.8}\text{Cu}_{0.2}\text{Cr}_2\text{O}_4$ (f) over the temperature range where structural and magnetic changes occur. The line features in the variable temperature data of sample $\text{Zn}_{0.8}\text{Cu}_{0.2}\text{Cr}_2\text{O}_4$ are due to slight temperature fluctuations during the measurement.

TABLE III: Magnetic parameters of $\text{Zn}_{1-x}\text{Cu}_x\text{Cr}_2\text{O}_4$.

	T_N (K)	$\mu_{exp}(\mu_B)$	$\mu_{calc}(\mu_B)$	Θ_{CW} (K)
ZnCr_2O_4	12.3	5.2	5.47	-288
$\text{Zn}_{0.9}\text{Cu}_{0.1}\text{Cr}_2\text{O}_4$	11	4.9	5.50	-239
$\text{Zn}_{0.8}\text{Cu}_{0.2}\text{Cr}_2\text{O}_4$	16	5.0	5.53	-270

in $\text{Zn}_{0.9}\text{Cu}_{0.1}\text{Cr}_2\text{O}_4$ and $\text{Zn}_{0.8}\text{Cu}_{0.2}\text{Cr}_2\text{O}_4$ at 45 K and 110 K respectively (middle panel of Fig. 8). The lattice distortions of $\text{Zn}_{0.9}\text{Cu}_{0.1}\text{Cr}_2\text{O}_4$ and $\text{Zn}_{0.8}\text{Cu}_{0.2}\text{Cr}_2\text{O}_4$ are shown by the divergence of the coincident (511) and (333) reflections at the respective distortion temperatures of these materials (Fig. 8). The structural changes of $\text{Zn}_{0.9}\text{Cu}_{0.1}\text{Cr}_2\text{O}_4$ and $\text{Zn}_{0.8}\text{Cu}_{0.2}\text{Cr}_2\text{O}_4$ are decoupled from antiferromagnetic ordering (Table III), nonetheless there is a change in slope of the inverse susceptibility of these systems at the structural distortion temperatures. Jahn-Teller distortion is enhanced in $\text{Zn}_{1-x}\text{Cu}_x\text{Cr}_2\text{O}_4$

with increase in Cu^{2+} content, occurring at higher temperatures and involving larger lattice distortions (Fig. 8). Like in $\text{Mg}_{1-x}\text{Cu}_x\text{Cr}_2\text{O}_4$, the Jahn-Teller phases of $\text{Zn}_{0.9}\text{Cu}_{0.1}\text{Cr}_2\text{O}_4$ [Fig. 9 (a)] and $\text{Zn}_{0.8}\text{Cu}_{0.2}\text{Cr}_2\text{O}_4$ [Fig. 9 (d)] are well modeled by the orthorhombic $Fddd$ space group. The complete structural descriptions of these compounds at room temperature and near 6 K are tabulated in Table VI of the appendix.

The large heat capacity anomaly of ZnCr_2O_4 at the spin-Jahn-Teller distortion temperature [Fig. 8 (d)] evolves into a broad transition in $\text{Zn}_{0.9}\text{Cu}_{0.1}\text{Cr}_2\text{O}_4$ [Fig. 8 (e)] and $\text{Zn}_{0.8}\text{Cu}_{0.2}\text{Cr}_2\text{O}_4$ [Fig. 8 (f)] over the temperature range where structural and magnetic changes take place.

We further explore the structural distortions of $\text{Zn}_{0.8}\text{Cu}_{0.2}\text{Cr}_2\text{O}_4$ by performing sequential Rietveld refinements from the high temperature cubic phase to the low temperature orthorhombic phase. The cubic lattice constant diverges into three independent orthorhombic

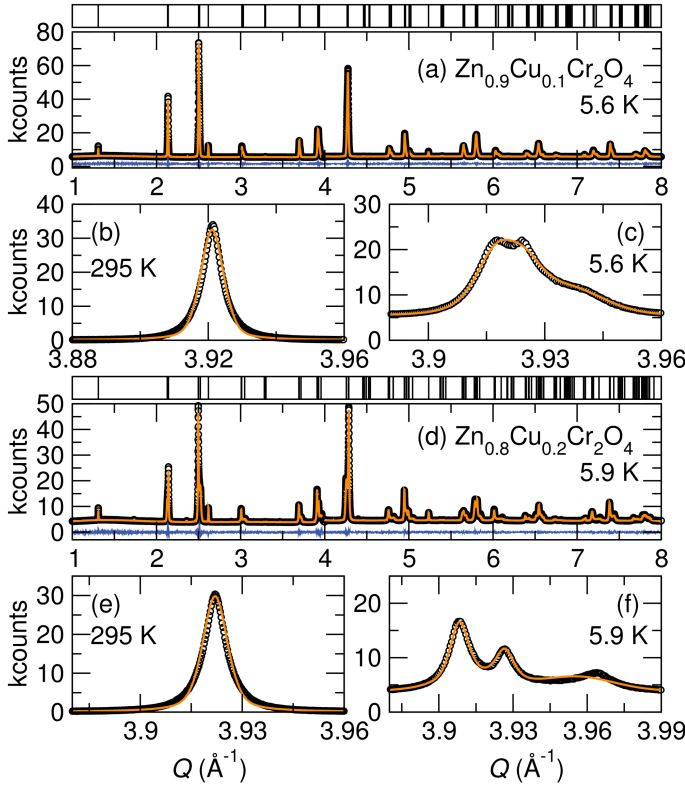


FIG. 9: (Color online) Synchrotron powder diffraction patterns of $\text{Zn}_{0.9}\text{Cu}_{0.1}\text{Cr}_2\text{O}_4$ (a) and $\text{Zn}_{0.8}\text{Cu}_{0.2}\text{Cr}_2\text{O}_4$ (d) collected near 6 K and indexed to the orthorhombic space group $Fddd$. Data is shown in black, the model is in orange while the difference is in blue. The high temperature coincident cubic $Fd\bar{3}m$ reflections (511) and (333) shown in (b) for $\text{Zn}_{0.9}\text{Cu}_{0.1}\text{Cr}_2\text{O}_4$ and in (e) for $\text{Zn}_{0.8}\text{Cu}_{0.2}\text{Cr}_2\text{O}_4$ are split at lower temperatures following the cubic to orthorhombic lattice distortion. These low temperature reflections as indexed to the orthorhombic $Fddd$ structure are shown in (c) and (f) for $\text{Zn}_{0.9}\text{Cu}_{0.1}\text{Cr}_2\text{O}_4$ and $\text{Zn}_{0.8}\text{Cu}_{0.2}\text{Cr}_2\text{O}_4$ respectively.

lattice parameters at 110 K [Fig. 10 (a)]. The a lattice constant decreases steeply with temperature while the b and c lattice constants increase. The orthorhombic distortion increases with decrease in temperature. Although the structural distortions of $\text{Mg}_{1-x}\text{Cu}_x\text{Cr}_2\text{O}_4$ and $\text{Zn}_{1-x}\text{Cu}_x\text{Cr}_2\text{O}_4$ occur primarily due to the Jahn-Teller activity of tetrahedral Cu^{2+} , there is a distinct difference in the distortions observed in the spinel solid solutions compared to the spinel CuCr_2O_4 . Jahn-Teller distortion in CuCr_2O_4 occurs near 853 K and involve a cubic $Fd\bar{3}m$ to tetragonal $I4_1/amd$ lattice distortion.³⁴ Magnetostructural coupling drives further structural distortion in CuCr_2O_4 from tetragonal $I4_1/amd$ to orthorhombic $Fddd$ symmetry.¹⁸ In the solid solutions $\text{Mg}_{1-x}\text{Cu}_x\text{Cr}_2\text{O}_4$ and $\text{Zn}_{1-x}\text{Cu}_x\text{Cr}_2\text{O}_4$, we observe a cubic $Fd\bar{3}m$ to orthorhombic $Fddd$ distortion, completely bypassing the tetragonal $I4_1/amd$ structure observed in CuCr_2O_4 and the lattice distortions occur without the onset of magnetic ordering. The different character of distortion in $\text{Mg}_{1-x}\text{Cu}_x\text{Cr}_2\text{O}_4$ and $\text{Zn}_{1-x}\text{Cu}_x\text{Cr}_2\text{O}_4$

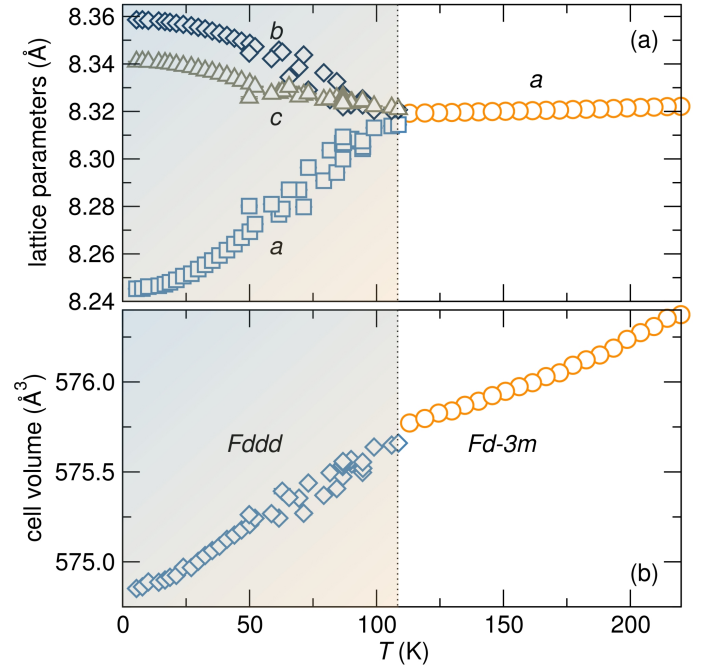


FIG. 10: (Color online) (a) The evolution of lattice parameters of $\text{Zn}_{0.8}\text{Cu}_{0.2}\text{Cr}_2\text{O}_4$ as a function of temperature revealing a structural distortion at 110 K where three orthorhombic $Fddd$ lattice constants emerge from the cubic $Fd\bar{3}m$ lattice constant. (b) There is a slight change in slope in the temperature dependent cell volume of $\text{Zn}_{0.8}\text{Cu}_{0.2}\text{Cr}_2\text{O}_4$ at the structural distortion temperature. Error bars are smaller than data symbols.

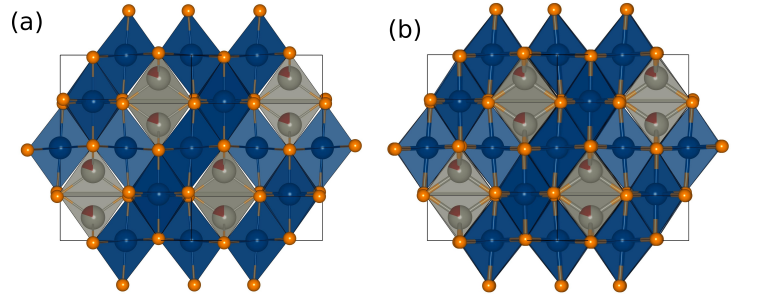


FIG. 11: (Color online) The spinel structure of $\text{Zn}_{0.8}\text{Cu}_{0.2}\text{Cr}_2\text{O}_4$ in the cubic $Fd\bar{3}m$ phase near 300 K and in the orthorhombic $Fddd$ phase near 6 K are shown in (a) and (b) respectively. Edge sharing CrO_6 (blue) octahedra are corner connected to $(\text{Zn/Cu})\text{O}_4$ (grey) tetrahedra. The shared (Zn/Cu) atomic site is shown in grey (Zn atomic fraction) and dark red (Cu atomic fraction). The ideal tetrahedral angle of 109.54° observed in the cubic phase (a) of $\text{Zn}_{0.8}\text{Cu}_{0.2}\text{Cr}_2\text{O}_4$ is distorted to two angles of 111.898° and 105.99° in the orthorhombic phase (b); the $(\text{Zn/Cu})\text{O}_4$ (grey) tetrahedra appear more flattened in the orthorhombic phase (b) filling the tetrahedral voids between the CrO_6 octahedra while small gaps can be seen between the $(\text{Zn/Cu})\text{O}_4$ (grey) tetrahedra and the CrO_6 (blue) octahedra in the cubic phase (a) of $\text{Zn}_{0.8}\text{Cu}_{0.2}\text{Cr}_2\text{O}_4$.

compared to CuCr_2O_4 is attributed to poor connectivity

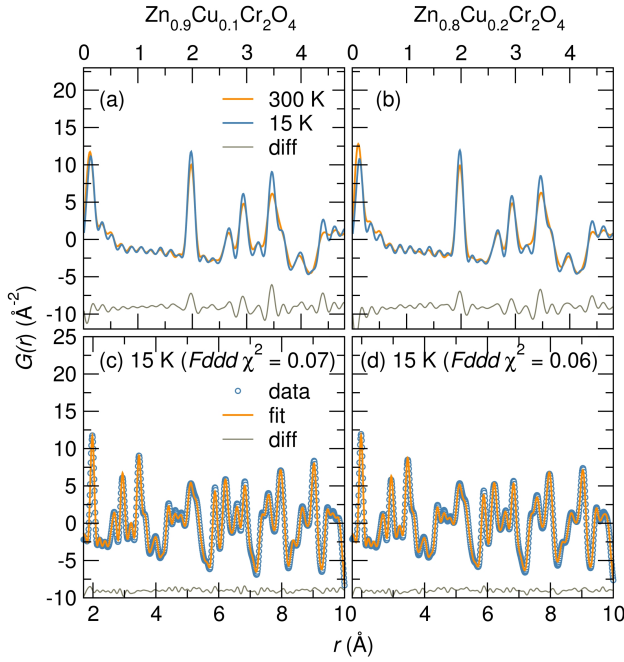


FIG. 12: (Color online) Pair distribution functions for $\text{Zn}_{0.9}\text{Cu}_{0.1}\text{Cr}_2\text{O}_4$ (a) and $\text{Zn}_{0.8}\text{Cu}_{0.2}\text{Cr}_2\text{O}_4$ (b) measured at 300 K and 15 K show that the local structure varies slightly from room temperature to low temperature. The low r region is shown in (a) and (b) to point out the slight increase in intensity of the pair distribution function at low temperature. The difference between the 15 K and the 300 K pair distribution functions is shown at the bottom. Least squares refinement of the pair distribution functions of these compounds at 15 K are well modeled by the $Fddd$ structure as shown in (c) and (d).

between CuO_4 tetrahedra. Dilute randomly distributed CuO_4 tetrahedra in the solid solutions results in average distortions in all axes of the unit cell and hence these systems adopt orthorhombic symmetry in the Jahn-Teller phases. Group-subgroup relations show that structural distortion from cubic $Fd\bar{3}m$ to orthorhombic $Fddd$ symmetry goes through an intermediate tetragonal $I4_1/amd$ space group. It is plausible that the Jahn-Teller ordering systems $\text{Mg}_{1-x}\text{Cu}_x\text{Cr}_2\text{O}_4$ and $\text{Zn}_{1-x}\text{Cu}_x\text{Cr}_2\text{O}_4$ quickly go through the tetragonal $I4_1/amd$ structure before adopting the orthorhombic structure. A similar cubic $Fd\bar{3}m$ to orthorhombic $Fddd$ lattice distortion driven by charge ordering has been observed in the cathode spinel material LiMn_2O_4 near room temperature.³⁶

The $\text{Zn}_{0.8}\text{Cu}_{0.2}\text{Cr}_2\text{O}_4$ unit cell contracts with decrease in temperature as reflected in Fig. 10 (b). There is a slight change in slope of the unit cell volume at the structural distortion temperature. This small change in slope of the cell volume at 110 K and the broad heat capacity anomaly of $\text{Zn}_{0.8}\text{Cu}_{0.2}\text{Cr}_2\text{O}_4$ suggest it undergoes a second-order structural distortion.

The AO_4 tetrahedra of the cubic phase of $\text{Zn}_{0.8}\text{Cu}_{0.2}\text{Cr}_2\text{O}_4$ are distorted in the orthorhombic phase. Specifically, a single A-O distance is preserved

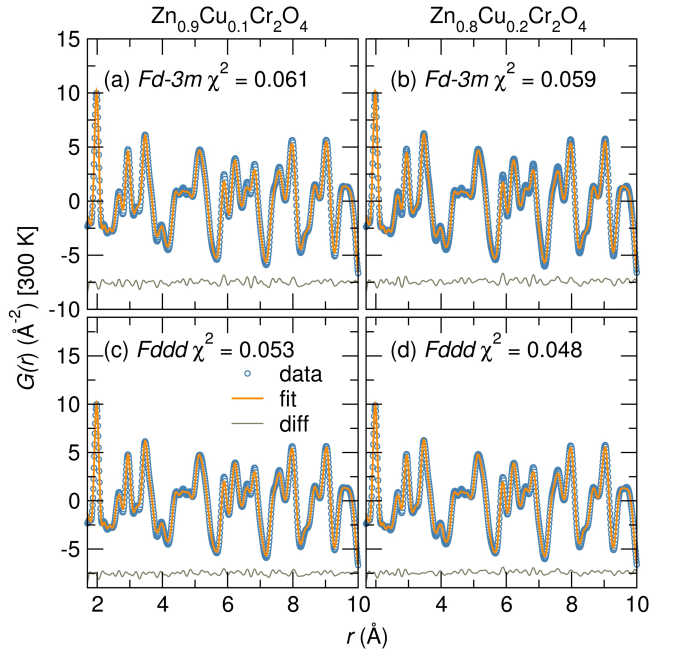


FIG. 13: (Color online) Least squares refinement of the pair distribution function of $\text{Zn}_{0.9}\text{Cu}_{0.1}\text{Cr}_2\text{O}_4$ and $\text{Zn}_{0.8}\text{Cu}_{0.2}\text{Cr}_2\text{O}_4$ collected at 300 K are indexed to the cubic $Fd\bar{3}m$ structure[(a) and (b)] and to the orthorhombic $Fddd$ structure[(c) and (d)]. A smaller difference curve and slightly better χ^2 parameters are obtained when the orthorhombic model is applied to the room temperature data suggesting that dynamic Jahn-Teller distortion may be present at ambient temperature that becomes static at the Jahn-Teller distortion temperatures of these compounds.

while two distinct O-A-O bond angles of 111.898° and 105.99° emerge from the ideal tetrahedral angle 109.47° of the cubic phase. The overall effect of these angle distortions in $\text{Zn}_{0.8}\text{Cu}_{0.2}\text{Cr}_2\text{O}_4$ is a compression of the tetrahedra. This is illustrated in Fig. 11 (a) where the ideal AO_4 tetrahedra of the cubic phase leave small voids in the surrounding CrO_6 network while the flattened AO_4 tetrahedra of the orthorhombic phase completely fill the tetrahedral voids [Fig. 11(b)]. The compression of AO_4 tetrahedra is similar to the flattening of CuO_4 tetrahedra in the orthorhombic phase of CuCr_2O_4 .¹⁸ The AO_4 distortions of $\text{Zn}_{0.8}\text{Cu}_{0.2}\text{Cr}_2\text{O}_4$ distort the surrounding CrO_6 matrix. Three distinct Cr-O bond distances and O-Cr-O bond angles emerge in the orthorhombic phase of $\text{Zn}_{0.8}\text{Cu}_{0.2}\text{Cr}_2\text{O}_4$ compared to the cubic phase where there are no bond length or bond angle distortions. The distortions of the Cr sublattice in $\text{Mg}_{1-x}\text{Cu}_x\text{Cr}_2\text{O}_4$ and $\text{Zn}_{1-x}\text{Cu}_x\text{Cr}_2\text{O}_4$ do not lift spin degeneracy and magnetic ordering in these materials still takes place below 20 K (Table II and III).

Real space structural descriptions of $\text{Zn}_{1-x}\text{Cu}_x\text{Cr}_2\text{O}_4$ for $x > 0$ give insights as to the nature of the Jahn-Teller distortions in these compounds. There are differences in the pair distribution functions of $\text{Zn}_{0.9}\text{Cu}_{0.1}\text{Cr}_2\text{O}_4$ and $\text{Zn}_{0.8}\text{Cu}_{0.2}\text{Cr}_2\text{O}_4$ collected at room temperature and at

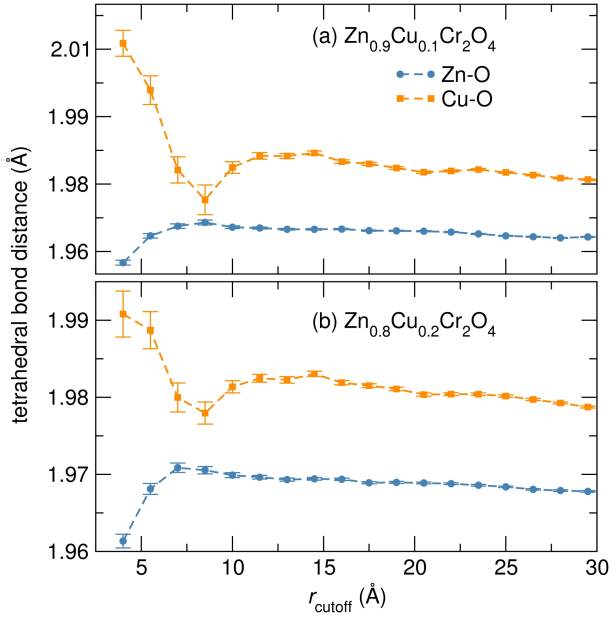


FIG. 14: (Color online) Least squares refinement of the pair distribution function of $\text{Zn}_{0.9}\text{Cu}_{0.1}\text{Cr}_2\text{O}_4$ (a) and $\text{Zn}_{0.8}\text{Cu}_{0.2}\text{Cr}_2\text{O}_4$ (b) to a two phase model of ZnCr_2O_4 and CuCr_2O_4 shows that the environment around Zn^{2+} varies from that around Cu^{2+} at low r as shown by the different Zn-O and Cu-O bond lengths of the ZnO_4 and CuO_4 tetrahedra. The phase fractions of the ZnCr_2O_4 model are 90% for $\text{Zn}_{0.9}\text{Cu}_{0.1}\text{Cr}_2\text{O}_4$ and 80% for $\text{Zn}_{0.8}\text{Cu}_{0.2}\text{Cr}_2\text{O}_4$. The differences in Zn-O and Cu-O bond lengths of the AO_4 tetrahedra are smaller at high r .

15 K as shown in Fig. 12 (a) and (b). The differences are mainly in the intensity of atom pair correlations; at low temperature, the distribution functions have slightly higher intensity than at room temperature where atomic vibrations broaden the pair distribution function [Fig. 12 (a) and (b)]. The low temperature average structural model, orthorhombic $Fddd$, describes the local structure of $\text{Zn}_{0.9}\text{Cu}_{0.1}\text{Cr}_2\text{O}_4$ and $\text{Zn}_{0.8}\text{Cu}_{0.2}\text{Cr}_2\text{O}_4$ at 15 K [Fig. 12 (c) and (d)].

Combined average and local structure studies can distinguish whether Jahn-Teller distortions occur spontaneously at the average structure distortion temperatures of $\text{Zn}_{0.9}\text{Cu}_{0.1}\text{Cr}_2\text{O}_4$ and $\text{Zn}_{0.8}\text{Cu}_{0.2}\text{Cr}_2\text{O}_4$ or whether local distortions of CuO_4 tetrahedra persist in the cubic phases of these materials with these distortions becoming cooperative at the Jahn-Teller distortion temperature. In Figure 13 we model the room temperature pair distribution functions of $\text{Zn}_{0.9}\text{Cu}_{0.1}\text{Cr}_2\text{O}_4$ (a) and $\text{Zn}_{0.8}\text{Cu}_{0.2}\text{Cr}_2\text{O}_4$ (b) to the cubic average structure model $Fd\bar{3}m$ and to the Jahn-Teller distorted orthorhombic $Fddd$ structure. At room temperature, the cubic $Fd\bar{3}m$ fit yields slightly larger goodness-of-fit parameters compared to the lower symmetry $Fddd$ fits [Fig. 13 (c) and (d)]. The better description of the local structure of these compounds at room temperature by the lower symmetry structural model suggests that local CuO_4 distor-

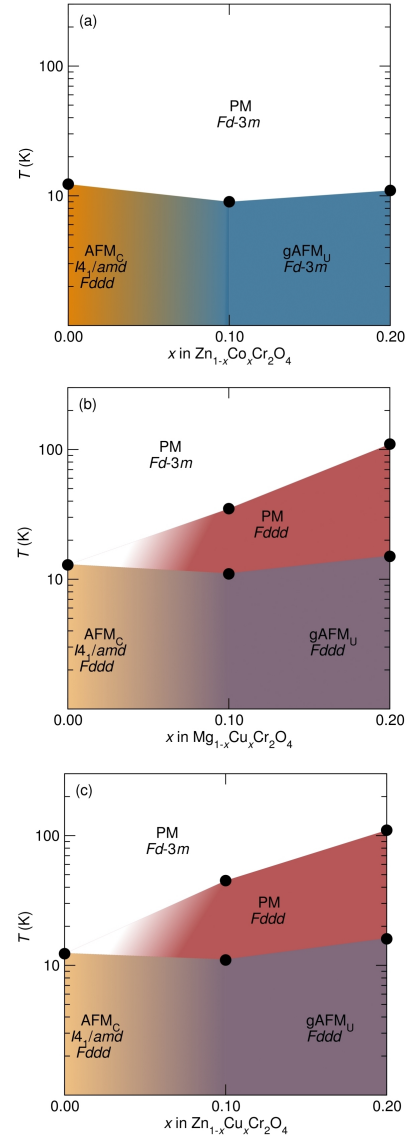


FIG. 15: (Color online) Temperature-composition phase diagrams of the spinel solid solutions $\text{Zn}_{1-x}\text{Co}_x\text{Cr}_2\text{O}_4$ (a), $\text{Mg}_{1-x}\text{Cu}_x\text{Cr}_2\text{O}_4$ (b), and $\text{Zn}_{1-x}\text{Cu}_x\text{Cr}_2\text{O}_4$ (c). At high temperatures all systems are paramagnetic (PM) and cubic in the space group $Fd\bar{3}m$. Magnetism evolves from frustrated compensated antiferromagnetism (AFM_C) in ZnCr_2O_4 and MgCr_2O_4 to glassy uncompensated antiferromagnetism (gAFM_U) when $x = 0.2$. A transition from cubic $Fd\bar{3}m$ to orthorhombic $Fddd$ symmetry occurs in $\text{Mg}_{1-x}\text{Cu}_x\text{Cr}_2\text{O}_4$ and $\text{Zn}_{1-x}\text{Cu}_x\text{Cr}_2\text{O}_4$ when $x \geq 0.1$ due to Jahn-Teller distortions of tetrahedral CuO_4 . We have recently reported that tetragonal $I4_1/amd$ and orthorhombic $Fddd$ structures coexist in the spin-Jahn-Teller phases of MgCr_2O_4 and ZnCr_2O_4 .⁶

tions are present in the cubic phases of $\text{Zn}_{0.9}\text{Cu}_{0.1}\text{Cr}_2\text{O}_4$ and $\text{Zn}_{0.8}\text{Cu}_{0.2}\text{Cr}_2\text{O}_4$ and that these distortions become cooperative at the respective Jahn-Teller distortion temperatures of these systems. The presence of local distortions in $\text{Zn}_{0.9}\text{Cu}_{0.1}\text{Cr}_2\text{O}_4$ and $\text{Zn}_{0.8}\text{Cu}_{0.2}\text{Cr}_2\text{O}_4$ is fur-

ther corroborated by least squares refinements of the pair distribution functions to a structural model of two cubic phases assigned to either ZnCr_2O_4 or CuCr_2O_4 [Fig. 14 (a) and (b)]. Structural models consisting of stoichiometrically weighted end-member structures have been previously successfully employed to describe the pair distribution function of the frustrated spinel $\text{CoAl}_{1.6}\text{Ga}_{0.4}\text{O}_4$ at low r .³⁷ In the two phase refinement, the ZnCr_2O_4 and CuCr_2O_4 structural models are scaled to correlate with the mole fractions of Zn^{2+} and Cu^{2+} and only the lattice parameters and $\text{Zn}^{2+}/\text{Cu}^{2+}$ thermal parameters are allowed to vary. There is a large difference in the Zn-O and Cu-O bond lengths in the two phases at low r_{cutoff} for both $\text{Zn}_{0.9}\text{Cu}_{0.1}\text{Cr}_2\text{O}_4$ and $\text{Zn}_{0.8}\text{Cu}_{0.2}\text{Cr}_2\text{O}_4$ and this difference decreases at high r_{cutoff} (Fig. 14). This suggests that there are local distortions in $\text{Zn}_{0.9}\text{Cu}_{0.1}\text{Cr}_2\text{O}_4$ and $\text{Zn}_{0.8}\text{Cu}_{0.2}\text{Cr}_2\text{O}_4$ that are best modeled by differentiating the environment around Zn^{2+} and Cu^{2+} . As one examines the pair distribution functions to higher r_{cutoff} , these local distortions are averaged out becoming less apparent as observed by the smaller difference in A-O bond lengths of ZnCr_2O_4 and CuCr_2O_4 . The presence of local distortions in $\text{Zn}_{0.9}\text{Cu}_{0.1}\text{Cr}_2\text{O}_4$ and $\text{Zn}_{0.8}\text{Cu}_{0.2}\text{Cr}_2\text{O}_4$ is in good agreement with total scattering studies of the spinels $\text{Mg}_{1-x}\text{Cu}_x\text{Cr}_2\text{O}_4$ by Shoemaker and Seshadri that show more distortions of the local CuO_4 environments compared to MgO_4 environments in this spinel solid solution.²⁰

Cu^{2+} substitution on the non-magnetic A sites of MgCr_2O_4 and ZnCr_2O_4 has very similar effects on the structure and magnetic properties of the resulting solid solutions. Average structure distortions due to Jahn-Teller ordering of CuO_4 tetrahedra occur in $\text{Mg}_{1-x}\text{Cu}_x\text{Cr}_2\text{O}_4$ and $\text{Zn}_{1-x}\text{Cu}_x\text{Cr}_2\text{O}_4$ without accompanying long-range magnetic ordering. The distortions of CuO_4 tetrahedra are present in the cubic phases of $\text{Zn}_{1-x}\text{Cu}_x\text{Cr}_2\text{O}_4$ when $x \geq 0.1$ and become cooperative at the Jahn-Teller distortion temperature where average structure distortions are observed. The Jahn-Teller distorted phases are described by the orthorhombic $Fddd$ space group. The degeneracy of Cr-Cr bond distances is broken when average structure distortions occur in $\text{Mg}_{1-x}\text{Cu}_x\text{Cr}_2\text{O}_4$ and $\text{Zn}_{1-x}\text{Cu}_x\text{Cr}_2\text{O}_4$, however, antiferromagnetic interactions remain largely frustrated with magnetic ordering occurring below 20 K. We contrast the propensity for Jahn-Teller distortions compared with spin-Jahn-Teller distortion in the systems $\text{Mg}_{1-x}\text{Cu}_x\text{Cr}_2\text{O}_4$ and $\text{Zn}_{1-x}\text{Cu}_x\text{Cr}_2\text{O}_4$ where only few Cu^{2+} cations drive Jahn-Teller distortions while these small concentrations of magnetic ions on the non-magnetic A sites of these materials completely suppress spin-Jahn-Teller distortion. The evolution of structure and magnetism in the solid solutions $\text{Zn}_{1-x}\text{Co}_x\text{Cr}_2\text{O}_4$, $\text{Mg}_{1-x}\text{Cu}_x\text{Cr}_2\text{O}_4$, and $\text{Zn}_{1-x}\text{Cu}_x\text{Cr}_2\text{O}_4$ are summarized in the phase diagrams presented in Fig. 15.

D. Conclusions

We report the effect of magnetic A site substitutions on spin and structural ordering in MgCr_2O_4 and ZnCr_2O_4 . We contrast the effect of $\text{Co}^{2+} 3d^7$ substitutions in $\text{Zn}_{1-x}\text{Co}_x\text{Cr}_2\text{O}_4$ with $\text{Cu}^{2+} 3d^9$ substitutions in $\text{Mg}_{1-x}\text{Cu}_x\text{Cr}_2\text{O}_4$ and $\text{Zn}_{1-x}\text{Cu}_x\text{Cr}_2\text{O}_4$. Spin disorder induced by $\text{Co}^{2+} 3d^7$ substitutions in $\text{Zn}_{1-x}\text{Co}_x\text{Cr}_2\text{O}_4$ suppress the spin-Jahn-Teller distortion of ZnCr_2O_4 . On the other hand, spin and lattice disorder due to $\text{Cu}^{2+} 3d^9$ substitutions in $\text{Mg}_{1-x}\text{Cu}_x\text{Cr}_2\text{O}_4$ and $\text{Zn}_{1-x}\text{Cu}_x\text{Cr}_2\text{O}_4$ induce Jahn-Teller distortions in the paramagnetic phases of these compounds yet antiferromagnetic interactions in these systems remain frustrated with long-range magnetic ordering occurring below 20 K with no accompanying structural transformations. In other words, the Jahn-Teller active Cu^{2+} ions decouple structural and magnetic ordering, even when only substituted in small amounts. The low-temperature nuclear structure of Cu^{2+} substituted MgCr_2O_4 and ZnCr_2O_4 is orthorhombic $Fddd$. Analysis of distortions in $\text{Zn}_{0.8}\text{Cu}_{0.2}\text{Cr}_2\text{O}_4$ indicate a flattening of AO_4 tetrahedra in the orthorhombic phase. Total neutron scattering studies of $\text{Zn}_{1-x}\text{Cu}_x\text{Cr}_2\text{O}_4$ suggest that AO_4 are likely distorted locally at room temperature with these distortions becoming cooperative where average structure distortions are observed. Addition of magnetic Co^{2+} and Cu^{2+} induce uncompensated antiferromagnetic interactions in $\text{Zn}_{1-x}\text{Co}_x\text{Cr}_2\text{O}_4$, $\text{Mg}_{1-x}\text{Cu}_x\text{Cr}_2\text{O}_4$, and $\text{Zn}_{1-x}\text{Cu}_x\text{Cr}_2\text{O}_4$. Compounds with dilute A site spins have broad heat capacity features suggesting remanent disorder in these materials. We find that spin-Jahn-Teller ordering is extremely sensitive to spin disorder while Jahn-Teller ordering is robust, and occurs even when only few Jahn-Teller active cations are substituted into the spinel structure.

E. Acknowledgements

This project was supported by the NSF through the DMR 1105301. MCK is supported by the Schlumberger Foundation Faculty for the Future fellowship. We acknowledge the use of shared experimental facilities of the Materials Research Laboratory: an NSF MRSEC, supported by NSF DMR 1121053. The 11-BM beamline at the Advanced Photon Source is supported by the DOE, Office of Science, Office of Basic Energy Sciences, under Contract No. DE-AC0206CH11357. This work benefited from the use of NPDF at the Los Alamos Neutron Scattering Center at Los Alamos National Laboratory, funded by DOE Office of Basic Energy Sciences; LANL is operated by Los Alamos National Security LLC under DE-AC52-06NA25396. MCK acknowledges helpful discussions with Jason E. Douglas and Brent C. Melot.

TABLE IV: Structural parameters of $\text{Zn}_{0.9}\text{Co}_{0.1}\text{Cr}_2\text{O}_4$ and $\text{Zn}_{0.8}\text{Co}_{0.2}\text{Cr}_2\text{O}_4$ obtained from Rietveld refinement of high-resolution synchrotron powder X-ray diffraction collected at 295 K and near 6 K and modeled to the cubic space group $Fd\bar{3}m$.

	$\text{Zn}_{0.9}\text{Co}_{0.1}\text{Cr}_2\text{O}_4$		$\text{Zn}_{0.8}\text{Co}_{0.2}\text{Cr}_2\text{O}_4$	
Temperature (K)	5.5	295	5.6	295
Setting	origin 2	origin 2	origin 2	origin 2
Z	8	8	8	8
$a(\text{\AA})$	8.32037(2)	8.327641(1)	8.32038(1)	8.327868(5)
Vol/ (\AA^3)	576.008(4)	577.519(3)	576.009(2)	577.566(1)
Zn/Co	$8a$ (1/8, 1/8 1/8)	$8a$ (1/8, 1/8, 1/8))	$8a$ (1/8, 1/8 1/8)	$8a$ (1/8, 1/8, 1/8)
U_{iso} (10^2\AA^2)	0.24(1)	0.389(5)	0.128(7)	0.398(5)
Cr	$16d$ (1/2, 1/2, 1/2)	$16d$ (1/2, 1/2, 1/2)	$16d$ (1/2, 1/2, 1/2)	$16d$ (1/2, 1/2, 1/2)
U_{iso} (10^2\AA^2)	0.196(9)	0.213(4)	0.145(6)	0.230(4)
O	$32h$ (x, y, z)	$32e$ (x, x, x)	$32h$ (x, y, z)	$32e$ (x, x, x)
	x 0.2612(1)	x 0.26205(4)	0.26208(7)	0.26221(5)
U_{iso} (10^2\AA^2)	0.54(3)	0.32(1)	0.35(2)	0.360(1)
χ^2	15.73	5.263	6.976	7.434
R_p (%)	8.10	9.12	7.54	9.33
R_{wp} (%)	10.12	11.54	9.43	12.56

TABLE V: Structural parameters of $\text{Mg}_{0.9}\text{Cu}_{0.1}\text{Cr}_2\text{O}_4$ and $\text{Mg}_{0.8}\text{Cu}_{0.2}\text{Cr}_2\text{O}_4$ obtained from Rietveld refinement of high-resolution synchrotron powder X-ray diffraction collected at 295 K and near 6 K.

	$\text{Mg}_{0.9}\text{Cu}_{0.1}\text{Cr}_2\text{O}_4$		$\text{Mg}_{0.8}\text{Cu}_{0.2}\text{Cr}_2\text{O}_4$	
	Orthorhombic	Cubic	Orthorhombic	Cubic
Temperature (K)	6.5	295	5.7	295
Space group	$Fddd$	$Fd\bar{3}m$	$Fddd$	$Fd\bar{3}m$
Setting	origin 2	origin 2	origin 2	origin 2
Z	8	8	8	8
$a(\text{\AA})$	8.293741(1)	8.332613(3)	8.231110(8)	8.330362(3)
$b(\text{\AA})$	8.335834(1)	8.332613(3)	8.360256(9)	8.330362(3)
$c(\text{\AA})$	8.3488(5)	8.332613(3)	8.373391(5)	8.330362(3)
Vol/ (\AA^3)	577.196(4)	578.554(1)	576.208(4)	578.085(1)
Mg/Cu	$8a$ (1/8, 1/8 1/8)	$8a$ (1/8, 1/8, 1/8))	$8a$ (1/8, 1/8 1/8)	$8a$ (1/8, 1/8, 1/8)
U_{iso} (10^2\AA^2)	0.384(2)	0.651(7)	0.371(2)	0.696(7)
Cr	$16d$ (1/2, 1/2, 1/2)	$16d$ (1/2, 1/2, 1/2)	$16d$ (1/2, 1/2, 1/2)	$16d$ (1/2, 1/2, 1/2)
U_{iso} (10^2\AA^2)	0.17(9)	0.321(3)	0.102(1)	0.344(3)
O	$32h$ (x, y, z)	$32e$ (x, x, x)	$32h$ (x, y, z)	$32e$ (x, x, x)
	x 0.26284(2)	x 0.26161(3)	0.260090(1)	0.26170(4)
	y 0.25845(3)	y 0.26161(3)	0.260627(2)	0.26170(4)
	z 0.262891(2)	z 0.26161(3)	0.263825(2)	0.26170(4)
U_{iso} (10^2\AA^2)	0.144(2)	0.651(7)	0.25(0)	0.59(1)
Cr_2O_3 wt%	0.89(8)	0.89(8)	0.87(7)	0.87(7)
χ^2	4.37	2.550	6.81	2.571
R_p (%)	6.7	5.98	6.29	6.23
R_{wp} (%)	9.16	8.12	8.14	8.15

TABLE VI: Structural parameters of $\text{Zn}_{0.9}\text{Cu}_{0.1}\text{Cr}_2\text{O}_4$ and $\text{Zn}_{0.8}\text{Cu}_{0.2}\text{Cr}_2\text{O}_4$ obtained from Rietveld refinement of high-resolution synchrotron powder X-ray diffraction collected at 295 K and near 6 K.

	$\text{Zn}_{0.9}\text{Cu}_{0.1}\text{Cr}_2\text{O}_4$		$\text{Zn}_{0.8}\text{Cu}_{0.2}\text{Cr}_2\text{O}_4$	
	Orthorhombic	Cubic	Orthorhombic	Cubic
Temperature (K)	5.6	295	5.9	295
Space group	$Fddd$	$Fd\bar{3}m$	$Fddd$	$Fd\bar{3}m$
Setting	origin 2	origin 2	origin 2	origin 2
Z	8	8	8	8
$a(\text{\AA})$	8.328150(7)	8.326101(6)	8.244895(8)	8.324244(7)
$b(\text{\AA})$	8.335862(5)	8.326101(6)	8.358441(5)	8.324244(7)
$c(\text{\AA})$	8.289697(5)	8.326101(6)	8.3409(1)	8.324244(7)
Vol/ (\AA^3)	575.490(3)	577.198(1)	574.809(5)	576.812(2)
Zn/Cu	$8a$ (1/8, 1/8 1/8)	$8a$ (1/8, 1/8, 1/8))	$8a$ (1/8, 1/8 1/8)	$8a$ (1/8, 1/8, 1/8)
U_{iso} (10^2\AA^2)	0.309(8)	0.455(5)	0.281(13)	0.470(5)
Cr	$16d$ (1/2, 1/2, 1/2)	$16d$ (1/2, 1/2, 1/2)	$16d$ (1/2, 1/2, 1/2)	$16d$ (1/2, 1/2, 1/2)
U_{iso} (10^2\AA^2)	0.297(8)	0.259(4)	0.254(13)	0.305(5)
O	$32h$ (x, y, z)	$32e$ (x, x, x)	$32h$ (x, y, z)	$32e$ (x, y, z)
	x 0.2577(3)	x 0.262015(47)	0.260315(184)	0.261641(53)
	y 0.2642(3)	y 0.262015(47)	0.266652(262)	0.261641(53)
	z 0.2628(2)	z 0.262015(47)	0.257599(340)	0.261641(53))
U_{iso} (10^2\AA^2)	0.329(21)	0.411(14)	0.304(33)	0.527(16)
Cr_2O_3 wt%	0.97(2)	0.97(2)	1.05(15)	1.05(15)
χ^2	4.494	6.582	7.808	7.805
R_p (%)	2.52	8.53	3.81	7.20
R_{wp} (%)	3.49	11.97	5.85	11.30

-
- * Electronic address: kemei@mrl.ucsb.edu
† Electronic address: seshadri@mrl.ucsb.edu
‡ Electronic address: suchomel@aps.anl.gov
§ Electronic address: dpshoema@illinois.edu
¶ Electronic address: kpage@lanl.gov
** Electronic address: siewienie@lanl.gov
- ¹ G. L. Pascut, R. Coldea, P. G. Radaelli, A. Bombardi, G. Beutier, I. I. Mazin, M. D. Johannes, and M. Jansen, *Phys. Rev. Lett.* **106**, 157206 (2011).
 - ² S.-H. Lee, C. Broholm, W. Ratcliff, G. Gasparovic, Q. Huang, T. H. Kim, and S.-W. Cheong, *Nature* **418**, 856 (2002).
 - ³ H. Ehrenberg, M. Knapp, C. Baehtz, and S. Klemme, *Powder Diff.* **17**, 230 (2002).
 - ⁴ L.-S. Martin, A. J. Williams, C. D. Gordon, S. Klemme, and J. P. Attfield, *J. Phys.: Condens. Matter* **20**, 104238 (2008).
 - ⁵ M. T. Rovers, P. P. Kyriakou, H. A. Dabkowska, G. M. Luke, M. I. Larkin, and A. T. Savici, *Phys. Rev. B* **66**, 174434 (2002).
 - ⁶ M. C. Kemei, P. T. Barton, S. L. Moffitt, M. W. Gaultois, J. A. Kurzman, R. Seshadri, M. R. Suchomel, and Y. Kim, *J. Phys.: Condens. Matter* **25**, 326001 (2013).
 - ⁷ A. P. Ramirez, *Annu. Rev. Mater. Sci.* **24**, 453 (1994).
 - ⁸ I. Kogomiya, H. Sawa, K. Siratori, K. Kohn, M. Toki, Y. Hata, and E. Kita, *Ferroelectrics* **268**, 327 (2002).
 - ⁹ J.-H. Chung, M. Matsuda, S.-H. Lee, K. Kakurai, H. Ueda, T. J. Sato, H. Takagi, K. P. Hong, and S. Park, *Phys. Rev. Lett.* **95**, 247204 (2005).
 - ¹⁰ R. V. Aguilar, A. B. Sushkov, Y. J. Choi, S. W. Cheong, and H. D. Drew, *Phys. Rev. B* **77**, 092412 (2008).
 - ¹¹ H. Ueda, H. Mitamura, T. Goto, and Y. Ueda, *Phys. Rev. B* **73**, 094415 (2006).
 - ¹² B. C. Melot, J. E. Drewes, R. Seshadri, E. M. Stoudenmire, and A. P. Ramirez, *J. Phys.: Condens. Matter* **21**, 216007 (2009).
 - ¹³ M. C. Kemei, S. L. Moffitt, D. P. Shoemaker, and R. Seshadri, *J. Phys.: Condens. Matter* **24**, 046003 (2012).
 - ¹⁴ L. Yan, F. Macia, Z. Jiang, J. Shen, L. He, and F. Wang, *J. Phys.: Condens. Matter* **20**, 255203 (2008).
 - ¹⁵ A. D. LaForge, S. H. Pulido, R. J. Cava, B. C. Chan, and A. P. Ramirez, *Phys. Rev. Lett.* **110**, 017203 (2013).
 - ¹⁶ S. E. Dutton, Q. Huang, O. Tchernyshyov, C. L. Broholm, and R. J. Cava, *Phys. Rev. B* **83**, 064407 (2011).
 - ¹⁷ R. D. Shannon, *Acta Crystallogr., Sect. A: Found. Crystallogr.* **32**, 751 (1976).
 - ¹⁸ M. R. Suchomel, D. P. Shoemaker, L. Ribaud, M. C. Kemei, and R. Seshadri, *Phys. Rev. B* **86**, 054406 (2012).
 - ¹⁹ P. T. Barton, R. Seshadri, A. Llobet, and M. R. Suchomel, *Phys. Rev. B* **88**, 024403 (2013).
 - ²⁰ D. P. Shoemaker and R. Seshadri, *Phys. Rev. B* **82**, 214107 (2010).
 - ²¹ B. H. Toby, *J. Appl. Crystallogr.* **34**, 210 (2001).
 - ²² A. C. Larson and R. B. V. Dreele, Los Alamos National Laboratory Report pp. 86–748 (2000).
 - ²³ K. Momma and F. Izumi, *J. Appl. Crystallogr.* **41**, 653 (2008).
 - ²⁴ P. F. Peterson, M. Gutmann, T. Proffen, and S. J. L. Billinge, *J. Appl. Crystallogr.* **33**, 1192 (2000).
 - ²⁵ C. L. Farrow, P. Juhas, J. W. Liu, D. Bryndin, E. S. Bozin, J. Bloch, T. Proffen, and S. J. L. Billinge, *J. Phys.: Condens. Matter* **19**, 335219 (2007).
 - ²⁶ S. Klemme and J. C. V. Miltenburg, *Mineral. Mag.* **68**, 515 (2004).
 - ²⁷ S.-H. Lee, G. Gasparovic, C. Broholm, M. Matsuda, J.-H. Chung, Y. J. Kim, H. Ueda, G. Xu, P. Zschack, K. Kakurai, et al., *J. Phys.: Condens. Matter* **19**, 145259 (2007).
 - ²⁸ N. Menyuk, K. Dwight, and A. Wold, *J. Phys.-Paris* **25**, 528 (1964).
 - ²⁹ K. Tomiyasu, J. Fukunaga, and H. Suzuki, *Phys. Rev. B* **70**, 214434 (2004).
 - ³⁰ G. Lawes, B. C. Melot, K. Page, C. Ederer, M. A. Hayward, T. Proffen, and R. Seshadri, *Phys. Rev. B* **74**, 024413 (2006).
 - ³¹ L. J. Chang, D. J. Huang, W.-H. Li, S.-W. Cheong, W. Ratcliff, and J. W. Lynn, *J. Phys.: Condens. Matter* **21**, 456008 (2009).
 - ³² V. Tsurkan, S. Zherlitsyn, S. Yasin, V. Felea, Y. Skourski, J. Deisenhofer, H.-A. K. von Nidda, J. Wosnitza, and A. Loidl, *Phys. Rev. Lett.* **110**, 115502 (2013).
 - ³³ N. Mufti, A. A. Nugroho, G. R. Blake, and T. T. M. Palstra, *J. Phys.: Condens. Matter* **22**, 075902 (2010).
 - ³⁴ Z.-G. Ye, O. Crottaz, F. Vaudano, F. Kubel, P. Tissot, and H. Schmid, *Ferroelectr. Lett.* **162**, 103 (1994).
 - ³⁵ E. Prince, *Acta Crystallogr., Sect. C: Cryst. Struct. Commun.* **10**, 554 (1957).
 - ³⁶ J. Rodriguez-Carvajal, G. Rousse, C. Masquelier, , and M. Hervieu, *Phys. Rev. Lett.* **81**, 4660 (1998).
 - ³⁷ B. C. Melot, K. Page, R. Seshadri, E. M. Stoudenmire, L. Balents, D. L. Bergman, and T. Proffen, *Phys. Rev. B* **80**, 104420 (2009).